iScience

CellPress
OPEN ACCESS

Article

circGlis3 promotes β-cell dysfunction by binding to heterogeneous nuclear ribonucleoprotein F and encoding Glis3-348aa protein

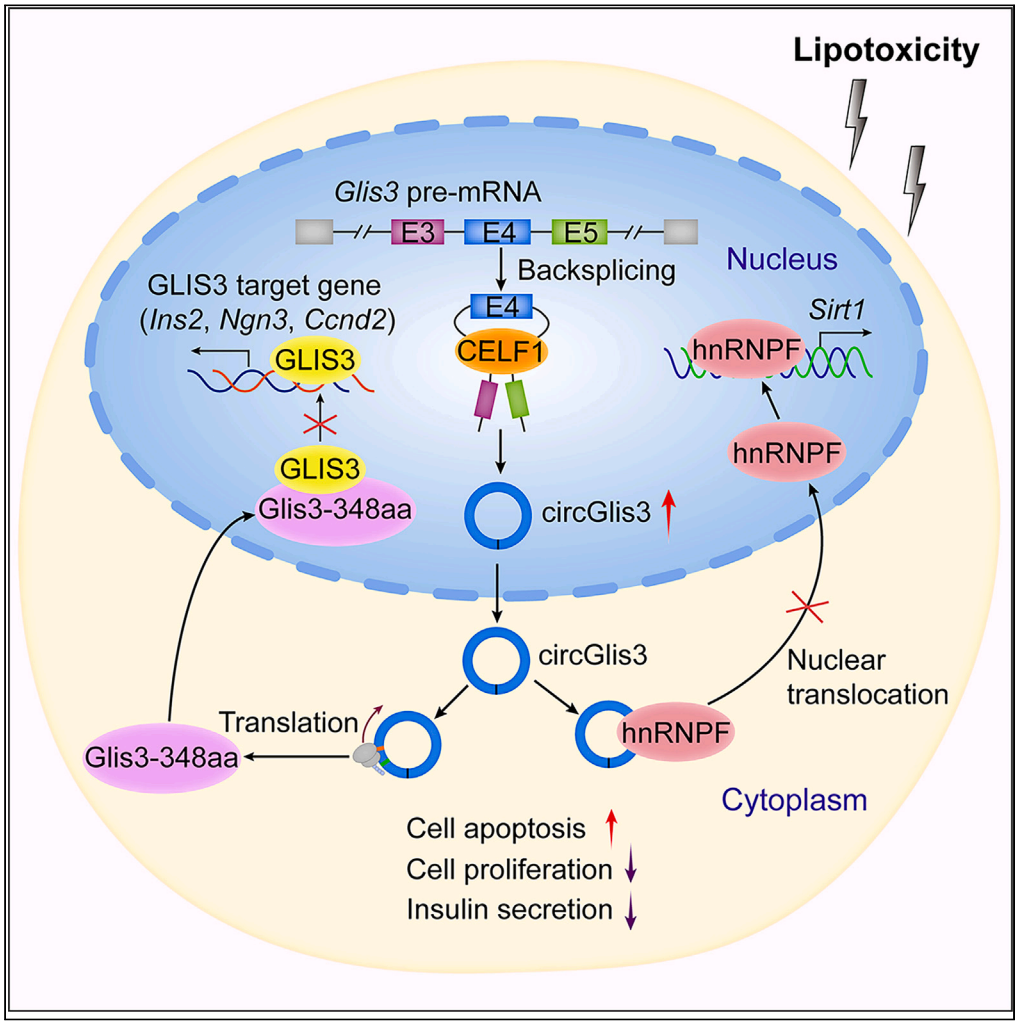

Li Xiong, Yingying Gong, Huashan Liu, ..., Wenxin Li, Zhenxing Liang, Liang Kang

liangzhx5@mail2.sysu.edu.cn (Z.L.)
kangl@mail.sysu.edu.cn (L.K.)

Highlights

The splicing factor CELF1 facilitates the biogenesis of circGlis3

Overexpression of circGlis3 promotes β-cell dysfunction *in vitro* and *in vivo*

CircGlis3 binds to hnRNPF protein and blocks its nuclear translocation

CircGlis3 encodes a 348aa protein to inhibit the transcriptional activity of GLIS3

Xiong et al., iScience *27*, 108680
January 19, 2024 © 2023 The Authors.
https://doi.org/10.1016/j.isci.2023.108680

iScience

CellPress
OPEN ACCESS

Article

circGlis3 promotes β-cell dysfunction by binding to heterogeneous nuclear ribonucleoprotein F and encoding Glis3-348aa protein

Li Xiong,[1,2,4] Yingying Gong,[3,4] Huashan Liu,[1,2] Liang Huang,[1,2] Ziwei Zeng,[1,2] Xiaobin Zheng,[1,2] Wenxin Li,[1,2] Zhenxing Liang,[1,2,*] and Liang Kang[1,2,5,*]

SUMMARY

Circular RNAs (circRNAs) are crucial regulators of β-cell function and are involved in lipotoxicity-induced β-cell damage in type 2 diabetes mellitus (T2DM). We previously identified that circGlis3, a circRNA derived from exon 4 of the diabetes susceptibility gene *Glis3*, was upregulated in lipotoxic β cells. However, the functional role and molecular mechanism of circGlis3 in β cells remain largely unknown. Here, we revealed that the splicing factor CUGBP Elav-Like Family Member 1 (CELF1) facilitated the biogenesis of circGlis3. Moreover, we established a transgenic mouse model and confirmed that the overexpression of circGlis3 impaired β-cell function. Mechanistically, circGlis3 bound to heterogeneous nuclear ribonucleoprotein F (hnRNPF) and blocked its nuclear translocation, thereby reducing *Sirt1* levels. Additionally, circGlis3 encoded a 348aa protein that interacted with GLIS3 and inhibited its transcriptional activity. Our data uncover a critical role of circGlis3 in β-cell dysfunction, suggesting that circGlis3 may be a potential therapeutic target for T2DM.

INTRODUCTION

Type 2 diabetes mellitus (T2DM) is a metabolic disorder syndrome characterized by insulin resistance and pancreatic β-cell failure.[1] The increase in T2DM prevalence is closely associated with obesity epidemics, and most patients with T2DM are obese or overweight with elevated circulating free fatty acids (FFAs), which are known as lipotoxicity.[2,3] Besides, β cells play a critical role in maintaining systemic glucose homeostasis, and lipotoxicity has been regarded as one of the major driving forces for insulin resistance and β-cell failure.[2,4] The molecular mechanisms of lipotoxic β-cell dysfunction include endoplasmic reticulum stress, mitochondrial dysfunction, and impaired autophagic flux.[5,6] Maintaining the functional integrity of β cells may delay the progression of diabetes. Therefore, a better understanding of the molecular mechanisms of β-cell failure under lipotoxic conditions is important for seeking new therapeutics for T2DM.

Studies have revealed that epigenetic mechanisms participate in the development of diabetes in multiple ways, including DNA methylation, histone modifications, and noncoding RNA (ncRNA) regulation.[7,8] Circular RNAs (circRNAs), a new class of ncRNAs with covalently closed loop structures, are involved in diverse cellular processes by acting as transcriptional regulators, microRNA (miRNA) sponges, anchors for RNA-binding proteins (RBPs) and sources of protein translation.[9,10] Moreover, circRNAs are expressed in a cell-type specific manner and may serve as promising biomarkers and therapeutic targets.[11–13] Accumulating data suggest that circRNAs are powerful regulators of β-cell function and are implicated in the progression of diabetes. For example, a recent study revealed an enriched circRNA profile in human islets, and found that four circRNAs (circCIRBP, circZKSCAN, circRPH3AL, and circCAMSAP1) were markedly associated with diabetes status.[14] Additionally, reduced levels of circHIPK3 and CDR1as in the islets of diabetic *db*/*db* mice had deleterious effects on β-cell survival and insulin secretion.[15] Similarly, circ-Tulp4, which was downregulated in the islets of *db*/*db* mice and lipotoxic MIN6 cells, inhibited β-cell proliferation by regulating miR-7222.[16] However, the functional roles of circRNAs in β cells and T2DM still remain elusive.

We previously reported that circGlis3 (mmu_circ_0000943), a circRNA generated from exon 4 of the *Glis3* gene, was upregulated in the islets of diabetic mice and in palmitate-treated MIN6 cells, and impaired β-cell function.[17] In this study, the underlying molecular mechanism

[1]Department of Colorectal Surgery, The Sixth Affiliated Hospital, Sun Yat-sen University, Guangzhou, Guangdong, China
[2]Department of General Surgery, Guangdong Provincial Key Laboratory of Colorectal and Pelvic Floor Diseases, The Sixth Affiliated Hospital, Sun Yat-sen University, Guangzhou, Guangdong, China
[3]Department of Geriatrics, The First Affiliated Hospital of Sun Yat-sen University, Guangzhou, Guangdong, China
[4]These authors contributed equally
[5]Lead contact
*Correspondence: liangzhx5@mail2.sysu.edu.cn (Z.L.), kangl@mail.sysu.edu.cn (L.K.)
https://doi.org/10.1016/j.isci.2023.108680

This is an open access article under the CC BY-NC-ND license (http://creativecommons.org/licenses/by-nc-nd/4.0/).

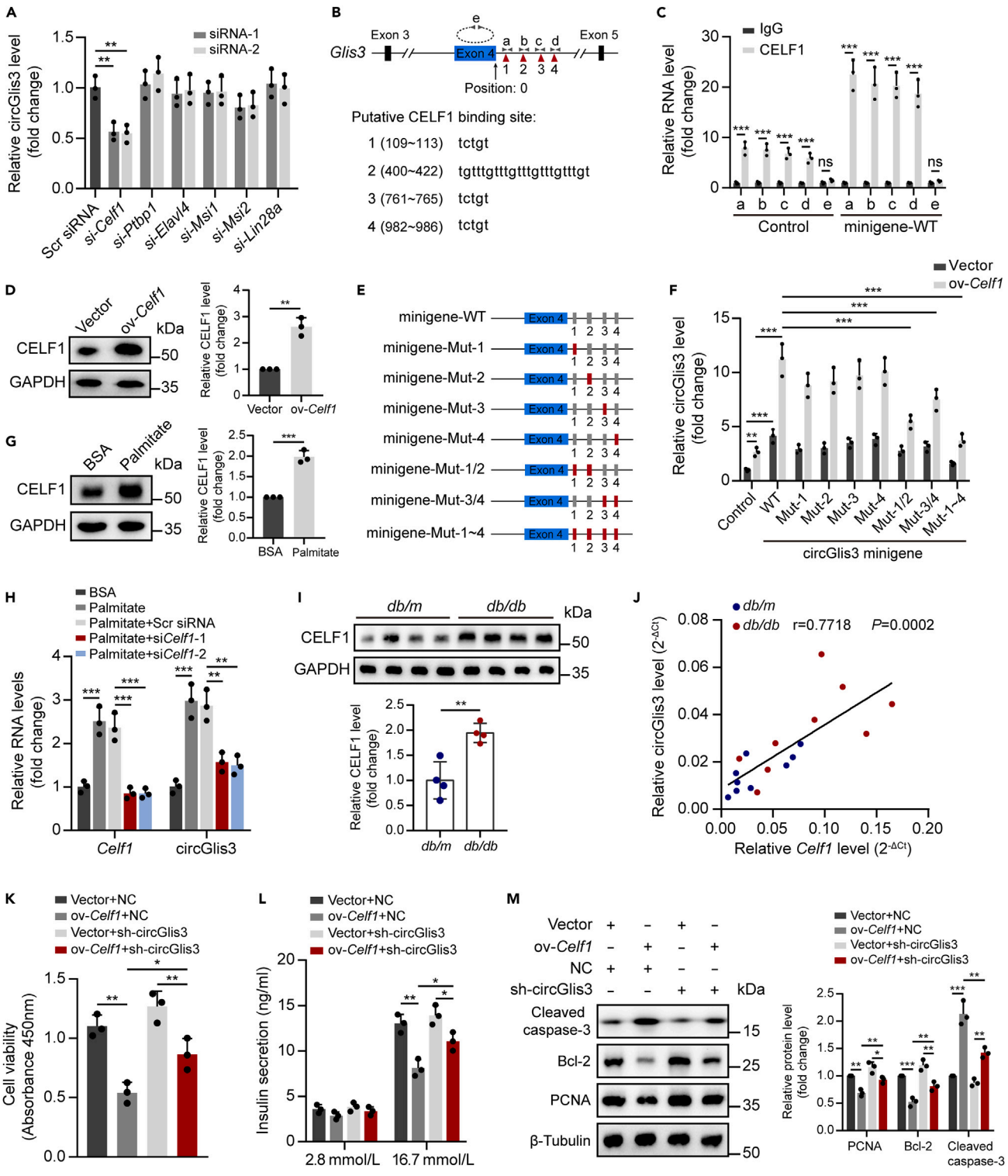

Figure 1. CELF1 promotes circGlis3 formation in β cells

(A) qRT-PCR analysis of the expression level of circGlis3 in MIN6 cells transfected with indicated siRNAs.

(B) Schematic of *Glis3* pre-mRNA showing the locations of four putative CELF1 binding sites (1–4) and amplicons (a–e) used for RIP assay.

(C) MIN6 cells were transfected with or without wild-type (WT) circGlis3 minigene, and then RIP assays were performed. The relative RNA levels of CELF1-binding fragments in circGlis3-flanked introns were analyzed by qRT-PCR using the primers indicated in (B). IgG served as a control.

Figure 1. *Continued*

(D) Western blot detected the protein levels of CELF1 in MIN6 cells transfected with *Celf1* plasmid (ov-*Celf1*) or empty vector (Vector).

(E) Schematic of circGlis3 minigenes with WT or mutant (Mut) CELF1 binding sites on the flanked intron regions of circGlis3.

(F) MIN6 cells were stably transfected with *Celf1* plasmid (ov-*Celf1*) or empty vector (Vector), and then transfected with WT or various mutant circGlis3 minigenes. qRT-PCR analyzed the expression level of circGlis3.

(G) Western blot analyzed CELF1 protein levels in MIN6 cells treated with 0.3 mmol/L palmitate or 0.3% BSA for 24 h.

(H) MIN6 cells with or without CELF1 knockdown were treated with 0.3 mmol/L palmitate, followed by qRT-PCR analysis of *Celf1* and circGlis3 levels.

(I) Western blot evaluated CELF1 protein levels in the islets of *db*/*db* and *db*/*m* mice (n = 4/group).

(J) Correlation between circGlis3 and *Celf1* in the islets of *db*/*db* and *db*/*m* mice was determined by qRT-PCR (n = 9/group). The statistical analysis was performed with Pearson's correlation analysis.

(K–M) MIN6 cells with or without CELF1 overexpression were transfected with shRNA targeting circGlis3 (sh-circGlis3) for rescue assays. Cell viability was detected by CCK-8 assay (K). Insulin secretion was assessed by GSIS assay (L). Western blot detected the expression levels of proteins (PCNA, Bcl-2 and Cleaved caspase-3) (M). The Western blots images are representative of three independent experiments unless otherwise noted. Data are represented as mean ± SD of three independent experiments. *$p < 0.05$, **$p < 0.01$ and ***$p < 0.001$, by two-tailed Student's *t* test in (C, D, G, and I), and one-way ANOVA (with Tukey post hoc test) in (A, F, H, and K–M).

by which circGlis3 promoted β-cell dysfunction was further explored. Our findings provide new insights into the role that circRNAs play in the pathophysiology of T2DM.

RESULTS

CUGBP Elav-like family member 1 regulates circGlis3 formation in β cells

Our previous study showed that circGlis3 levels in β cells were elevated by lipotoxicity, leading to β-cell dysfunction.[17] Here, we sought to explore the molecular mechanisms driving circGlis3 upregulation in β cells. It has been revealed that splicing factors participate in regulating circRNAs biogenesis by binding to the flanked intron regions.[18,19] To identify splicing factors involved in circGlis3 biogenesis, the RBPs likely to bind to the circGlis3 flanking intronic regions were predicted using the catRAPID omics web server, a tool for characterizing RNA-protein interactions.[20] A total of 22 RBPs were predicted to be most likely to bind to the flanking sequence within 1000 bp proximal to the back-splicing site of circGlis3 (Figure S1A). Besides, it is reasonable to postulate that if a splicing factor contributes to circGlis3 formation, it would also be dysregulated in diabetic β cells. Based on this hypothesis, we reviewed the literature,[21–25] and identified 26 RBPs that were dysregulated in diabetes and played a role in β cells (see Table S1). These proteins were overlapped with RBPs predicted by the catRAPID omics web server, and six proteins were left (Figure S1B). Therefore, we focused on the following RBPs: CELF1, PTBP1, ELAVL4, MSI1, MSI2, and LIN28A. Then, siRNAs were used to knockdown these RBPs individually, and the expression level of circGlis3 was assessed. The results showed that the silencing of CELF1 resulted in the downregulation of circGlis3 but not linear *Glis3* mRNA, suggesting that CELF1 was a key protein for circGlis3 biogenesis (Figures 1A, S1C, and S1D). Similarly, knockdown of CELF1 decreased circGlis3 levels, while the overexpression of CELF1 increased circGlis3 levels in primary mouse islets (Figure S1E). CELF1, a multifunctional RBP associated with RNA metabolism processes, binds to GU-rich element in pre-mRNA and affects splice site selection.[26] We further examined whether CELF1-binding sequences on the flanked intron regions were required for the biogenesis of circGlis3. Four putative CELF1-binding sites were identified downstream of the circGlis3-forming splice site (Figure 1B). Then, a circGlis3 minigene was constructed, and RNA immunoprecipitation (RIP) assays were performed in MIN6 cells and primary islets. As shown in Figures 1C and S1F, the enrichment of the four putative CELF1-binding sites was higher in the anti-CELF1 group than in the anti-IgG group, and the transfection of circGlis3 minigene further improved the enrichment, whereas binding to the circGlis3 itself was negligible, indicating that CELF1 could bind to circGlis3 minigene.

We further constructed a stable β cell line with CELF1 overexpression and a series of circGlis3 minigenes with CELF1-binding site mutations (Figures 1D and 1E). To evaluate the transfection efficiency of various constructs, a GFP tag was inserted into the minigene vector and GFP fluorescence intensity in MIN6 cells was analyzed by flow cytometry. The results showed that there was no significant difference in the mean fluorescence intensity (MFI) among MIN6 cells transfected with various minigenes (Figure S1G). Notably, the overexpression of CELF1 enhanced circGlis3 levels, and the mutation of any of the putative binding sites individually had little effect on the expression of circGlis3, while mutation of all four CELF1-binding sites substantially reduced circGlis3 formation (Figure 1F). Additionally, RIP assays showed that compared with minigene-WT, minigene-Mut failed to improve the enrichment of CELF1-binding sites, indicating that CELF1 had a significant interaction with minigene-WT, but not minigene-Mut (Figure S1H). These results suggest that these four CELF1-binding sites on the downstream flanked intron regions of circGlis3 are necessary for CELF1-mediated circGlis3 circularization.

Moreover, CELF1 levels in MIN6 cells were significantly increased by palmitate, whereas silenced by the transfection of siRNAs (Figures 1G and 1H). Consistently, circGlis3 levels in MIN6 cells were elevated by lipotoxicity, whereas decreased by knockdown of CELF1 (Figure 1H). Likewise, CELF1 was upregulated in the islets of *db*/*db* mice compared to *db*/*m* mice, and the mRNA level of *Celf1* was positively correlated with the circGlis3 expression level in mouse islets (Figures 1I and 1J). The expression level of *Glis3* pre-mRNA in palmitate-treated MIN6 cells was not significantly increased, which ruled out the possibility that the elevation of the circGlis3 level was affected by the increased level of *Glis3* pre-mRNA (Figure S1I). Additionally, the overexpression of CELF1 reduced cell viability, insulin secretion, and proliferation in MIN6 cells, whereas increased cell apoptosis, which could be partly rescued by silencing circGlis3 (Figures 1K–1M). Similar results were observed in primary mouse islets (Figures S1J and S1K). Altogether, these data indicate that lipotoxicity upregulates the expression level of CELF1, which promotes the biogenesis of circGlis3 in β cells.

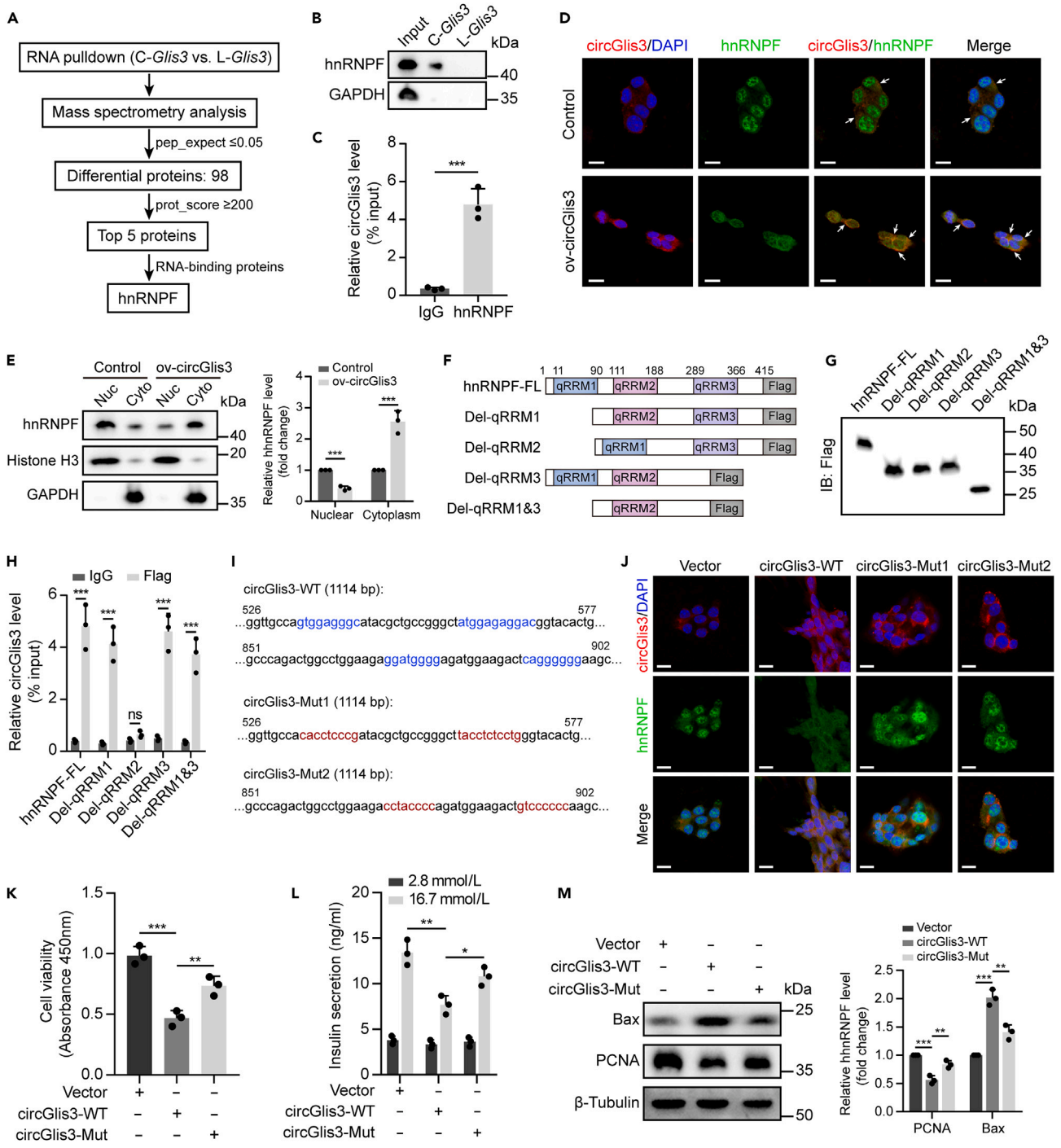

Figure 2. CircGlis3 binds to hnRNPF and inhibits its nuclear translocation

(A) Biotin-labeled circGlis3 probe (C-Glis3) and linear RNA probe with an identical sequence as circGlis3 (L-Glis3) were *in vitro* transcribed, then total protein of MIN6 cells was collected and RNA pulldown assay was performed. Flowchart illustrating the screening process for potential circGlis3-binding proteins.

(B) Western blot detected hnRNPF levels in the samples pulled down by circular (C-*Glis3*) or linear (L-*Glis3*) RNA probe.

(C) RIP assay was performed using anti-hnRNPF antibody, followed by qRT-PCR to detect circGlis3 enrichment.

(D) Dual RNA-FISH and IF verified the colocalization of circGlis3 and hnRNPF in MIN6 cells. Scale bar, 10 μm.

(E) Western blot analyzed the distribution of hnRNPF in the nucleus and cytoplasm of MIN6 cells with circGlis3 overexpression. GAPDH and Histone H3 were used as cytoplasmic and nuclear protein control, respectively (F) Schematic diagram showing the construction of Flag-tagged hnRNPF plasmids with full-length (FL) or different forms of truncation.

Figure 2. *Continued*

(G and H) MIN6 cells were transfected with plasmids encoding Flag-tagged FL or truncated hnRNPFs. Western blot verified the expression of Flag-tagged recombinant hnRNPF protein (G). RIP-qPCR assay using anti-Flag antibody was performed to detect the enrichment of circGlis3 (H).

(I) Schematic illustration of WT circGlis3 plasmid (circGlis3-WT) and circGlis3 plasmids with mutated RNA-binding motifs of hnRNPF within 526–577 bp (circGlis3-Mut1) or 851–902 bp (circGlis3-Mut2).

(J) Dual RNA-FISH and IF analyzed the expression of circGlis3 and the distribution of hnRNPF in MIN6 cells transfected with the plasmids indicated in (I). Scale bar, 10 μm.

(K–M) A mutant circGlis3 plasmid (circGlis3-Mut) was constructed by mutating the RNA-binding motifs of hnRNPF within 526–577 bp and 851–902 bp. MIN6 cells were transfected with circGlis3-WT or circGlis3-Mut plasmid. Cell viability was measured by CCK-8 assay (K). Insulin secretion was assessed by GSIS assay (L). Western blot detected the expression levels of PCNA and Bax (M). The Western blots images are representative of three independent experiments. Data are expressed as mean ± SD of three independent experiments. *$p < 0.05$, **$p < 0.01$ and ***$p < 0.001$, ns indicates no statistical significance, by two-tailed Student's *t* tests in (C, E, H), and one-way ANOVA (with Tukey post hoc test) in (K–M).

CircGlis3 directly interacts with heterogeneous nuclear ribonucleoprotein F and inhibits its nuclear translocation

Next, we investigated the underlying mechanism by which circGlis3 damaged β-cell function. Increasing data have demonstrated that circRNAs could function by interacting with proteins.[27,28] Therefore, RNA pulldown assay followed by MS analysis were performed to identify the protein partner of circGlis3 in β cells. 98 circGlis3-interacting proteins in MIN6 cells were identified, among which heterogeneous nuclear ribonucleoprotein F (hnRNPF) was ranked as one of the top five highest counts and belonged to RNA-binding proteins (Figures 2A and S2A; Table S2). The presence of hnRNPF in the circGlis3 probe pull-down sample was further confirmed by Western blot (Figure 2B). RIP assays in MIN6 cells and primary mouse islets verified the endogenous enrichment of circGlis3 in hnRNPF antibody co-precipitated RNA (Figures 2C and S2B). Dual RNA-FISH and immunofluorescence (IF) assay demonstrated the colocalization of circGlis3 and hnRNPF in MIN6 cells (Figure 2D). In addition, we noticed that hnRNPF protein levels were decreased in the nucleus and increased in the cytoplasm after overexpressing circGlis3 in MIN6 cells and islets, while modifying circGlis3 levels had no significant effect on the total protein level of hnRNPF (Figures 2D, 2E, S2C, and S2D). Similarly, the islets of *db/db* diabetic mice displayed reduced hnRNPF protein levels in the nucleus and increased hnRNPF protein levels in the cytoplasm (Figure S2E). These data indicate that the binding of circGlis3 to hnRNPF prevents the nuclear translocation of hnRNPF.

Subsequently, we examined the domain where hnRNPF binds to circGlis3. Flag-tagged hnRNPF plasmids with full-length or different forms of truncation were constructed and transfected into MIN6 cells (Figures 2F and 2G). *In vitro* binding assays showed that the quasi-RNA recognition motif 2 (qRRM2) of hnRNPF was essential for its interaction with circGlis3 (Figure 2H). Moreover, based on the RNA-binding motifs of hnRNPF and the online catRAPID algorithm, hnRNPF was predicted to likely bind to the 526–577 bp and 851–902 bp of circGlis3 (Figure S2F). Wild-type (WT) and mutant circGlis3 plasmids were designed and transfected into MIN6 cells. IF assay and Western blot revealed that mutating the RNA-binding motifs of hnRNPF within 526–577 bp of circGlis3 (circGlis3-Mut1) and 851–902 bp of circGlis3 (circGlis3-Mut2) could abolish the effect of circGlis3 on the subcellular distribution of hnRNPF, indicating that 526–577 bp and 851–902 bp of circGlis3 were indispensable for hnRNPF recruitment (Figures 2I, 2J, and S2G). A mutant circGlis3 plasmid (circGlis3-Mut) was further constructed by simultaneously mutating the RNA-binding motifs of hnRNPF within 526–577 bp and 851–902 bp of circGlis3. The results showed that compared with circGlis3-WT, circGlis3-Mut had little effect on β-cell viability, insulin secretion, proliferation, and apoptosis (Figures 2K–2M, S2H, and S2I). These findings collectively suggest that circGlis3 binds to the qRRM2 motif of hnRNPF through the 526–577 bp and 851–902 bp regions, thereby inhibiting the nuclear translocation of hnRNPF in β cells.

CircGlis3 induces β-cell dysfunction by disrupting the heterogeneous nuclear ribonucleoprotein F/Sirtuin 1 signaling pathway

hnRNPF belongs to the hnRNP family, which consists of RNA-binding nuclear proteins associated with nucleic acid metabolism.[29] Studies have shown that hnRNPF participated in kidney injury in diabetic mice.[30,31] To further elucidate the functional roles of hnRNPF in β cells, hnRNPF was knocked down using siRNAs (Figure 3A). Silencing hnRNPF significantly reduced cell viability and proliferation, inhibited insulin secretion, and increased cell apoptosis in MIN6 cells and islets, suggesting an important role of hnRNPF in regulating β-cell function (Figures 3B–3F and S3A–S3C). Moreover, hnRNPF has been reported to modulate the transcription of a series of genes in diabetic nephropathy, including *Sirtuin 1* (*Sirt1*), *Ace-2*, *Nrf2,* and *Bcl2-modifying factor* (*Bmf*), by binding to corresponding promoters in the nucleus.[31–34] Considering that the promoter DNA sequences are essentially the same in different cells of the same organism, we thus wondered if circGlis3 could affect the transcription levels of these genes by reducing the nuclear hnRNPF protein levels in β cells. Therefore, the levels of *Sirt1*, *Ace2*, *Nrf2,* and *Bmf* in response to the overexpression of circGlis3 were detected. The results showed that only *Sirt1* levels were noticeably decreased by overexpressing circGlis3 in MIN6 cells and islets, while the expression of other genes did not change significantly (Figures 3G, S3D, and S3E). Consistently, the expression level of *Sirt1* in β cells was reduced by silencing hnRNPF and increased by overexpressing hnRNPF (Figures 3H, S3F, and S3G). Dual-luciferase reporter assays confirmed that hnRNPF stimulated the *Sirt1* promoter activity in MIN6 cells (Figure 3I). We further constructed luciferase plasmids containing various lengths of the *Sirt1* gene promoter and co-transfected them with hnRNPF expression vectors into MIN6 cells. The activity of *Sirt1* promoters (N-1000/+100, N-500/+100, and N-250/+100) increased significantly compared with the control group, whereas the deletion of nucleotides N-1000 to N-25 (N-25/+100) markedly reduced *Sirt1* promoter activity, indicating that hnRNPF mainly binds to the N-250 to N-25 region of *Sirt1* promoter to promote *Sirt1* transcription in β cells (Figure 3J).

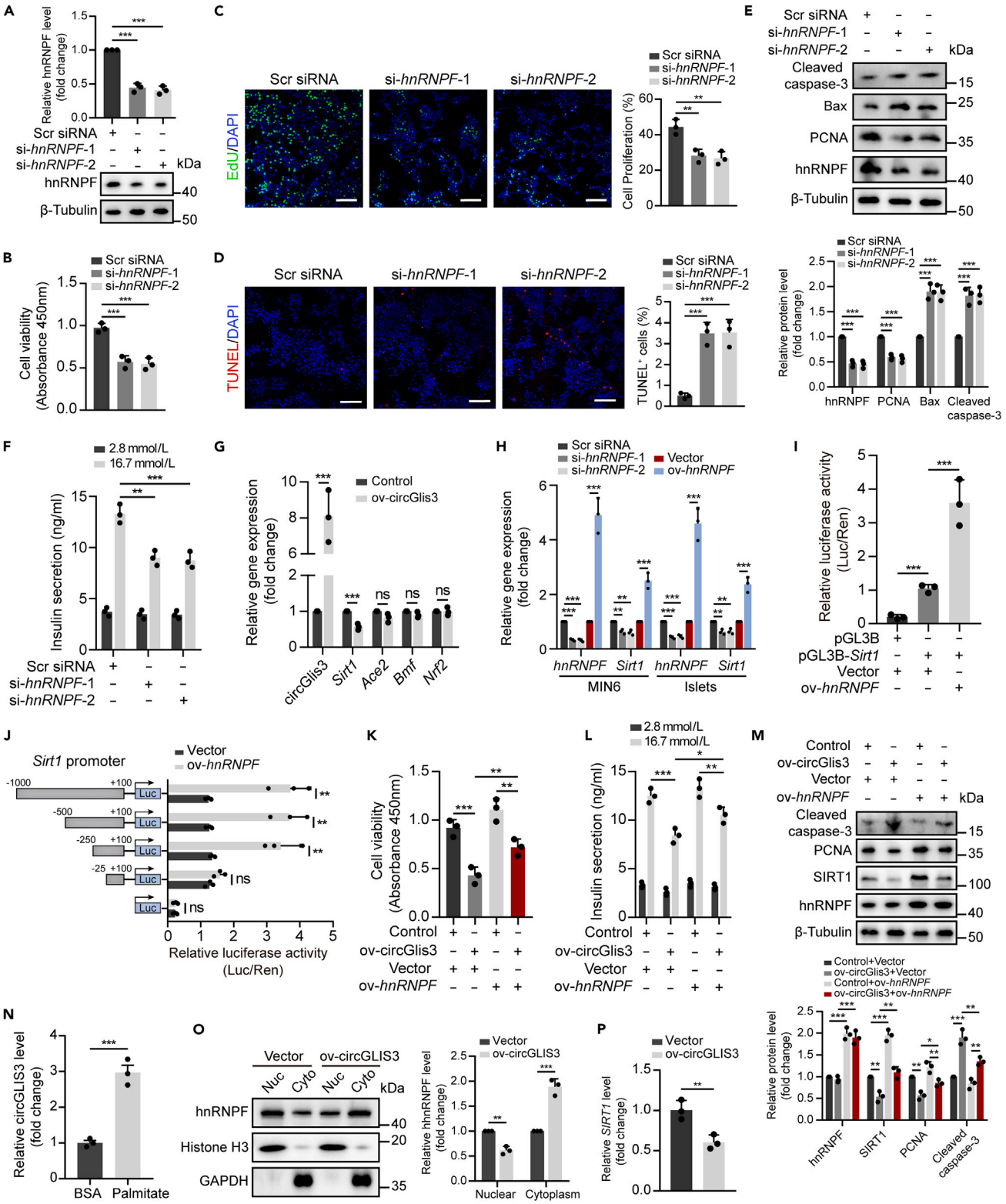

Figure 3. CircGlis3 induces β-cell dysfunction by disrupting the hnRNPF/SIRT1 pathway

(A–F) Scramble siRNA or siRNAs targeting *hnRNPF* (si-*hnRNPF*-1 and si-*hnRNPF*-2) were transfected into MIN6 cells for 48 h. Western blot detected the protein levels of hnRNPF (A). Cell viability was assessed by CCK-8 assay (B). Cell proliferation was determined by EdU staining. Scale bar, 100 μm (C). Cell apoptosis was

Figure 3. *Continued*

evaluated by TUNEL staining. Scale bar, 100 μm (D). The expression levels of proteins (hnRNPF, PCNA, Bax and Cleaved caspase-3) were analyzed by Western blot (E). Insulin secretion was assessed by GSIS assay (F).

(G) qRT-PCR analysis of the expression levels of circGlis3, *Sirt1*, *Ace2*, *Nrf2* and *Bmf* in MIN6 cells with circGlis3 overexpression.

(H) qRT-PCR detected the levels of *hnRNPF* and *Sirt1* in MIN6 cells and primary islets with hnRNPF overexpression or knockdown.

(I) Luciferase (Luc) activities of MIN6 cells co-transfected with luciferase reporter vector containing the *Sirt1* gene promoter and pcDNA-*hnRNPF* plasmid or empty vector. Data were normalized by co-transfecting the Renilla luciferase (Rluc) reporter vector.

(J) Luciferase activities of MIN6 cells co-transfected with plasmids containing various lengths of the *Sirt1* gene promoter and hnRNPF overexpression vector or empty vector.

(K–M) MIN6 cells with circGlis3 overexpression were transfected with pcDNA-*hnRNPF* plasmid (ov-*hnRNPF*) or empty vector (Vector) for rescue assays. Cell viability was analyzed by CCK-8 assay (K). Insulin secretion was measured by GSIS assay (L). Western blot detected the protein levels of hnRNPF, SIRT1, PCNA and Cleaved caspase-3 (M).

(N) qRT-PCR detected the levels of circGLIS3 in NES2Y cells treated with 0.3 mmol/L palmitate or 0.3% BSA for 24 h.

(O and P) NES2Y cells were transfected with empty vector or circGLIS3 plasmid. Western blot analyzed the distribution of hnRNPF in the nucleus and cytoplasm of NES2Y cells (O). qRT-PCR measured the expression levels of SIRT1 in NES2Y cells (P). Values are represented as mean ± SD of three independent experiments. *$p < 0.05$, **$p < 0.01$ and ***$p < 0.001$, ns indicates no significance, by two-tailed Student's *t* test in (G, J, N-P), and one-way ANOVA (with Tukey post hoc test) in (A–F, H, I, and K–M).

We next determined whether circGlis3 regulates β-cell function through the hnRNPF/SIRT1 axis. As anticipated, overexpression of circGlis3 decreased β-cell viability, proliferation, and insulin secretion, whereas increased cell apoptosis, which were ameliorated by elevating hnRNPF levels (Figures 3K, 3L, S3H, and S3I). Meanwhile, overexpressing circGlis3 reduced the protein levels of SIRT1 and proliferating cell nuclear antigen (PCNA) in β cells, whereas elevated the levels of Cleaved caspase-3, which could be rescued by overexpressing hnRNPF (Figures 3M and S3J). In addition, human pancreatic β cell line NES2Y was used to confirm the functional role of human circGLIS3 in β cells. The results showed that circGLIS3 was significantly upregulated in palmitate-treated NES2Y cells, and overexpression of circGLIS3 in NES2Y cells decreased hnRNPF protein levels in the nucleus and increased its levels in the cytoplasm (Figures 3N and 3O). Consistently, SIRT1 levels in NES2Y cells were reduced by overexpressing circGLIS3 (Figure 3P). Overall, our data illustrate that circGlis3 exerts its detrimental impacts on β cells, at least partly, through the hnRNPF/SIRT1 pathway.

CircGlis3 encodes a 348-amino acid (aa) protein

Accumulating evidence suggests that circRNAs have protein-coding potential and that the circRNA-encoded proteins participate in multiple physiological behaviors.[18,35] Interestingly, we noticed that eukaryotic translation initiation factor 2 subunit 1 (EIF2S1), a protein involved in protein translation, was detected in circGlis3 probe pull-down samples, and the presence of EIF2S1 was verified by Western blot (Figures S4A and S4B; Table S2). RIP assay further confirmed the interaction between circGlis3 and EIF2S1 (Figure 4A). Moreover, polysome profiling assay observed the co-sediments of circGlis3 and polysomes, suggesting that circGlis3 may be translated (Figure 4B). The co-sediments were also found in *Actin* mRNA, but not circPms1 (Figures 4C and 4D). Inspection of the circGlis3 sequence revealed the presence of an open reading frame (ORF) with a start codon and an internal ribosome entry site (IRES) (Figure 4E). We next evaluated the putative IRES activity in circGlis3 using dual-luciferase assays. The sequences of WT, truncated or mutated IRES were amplified and inserted between tandem RLuc and Luc reporters with independent start and stop codons (Figure 4F). The details of the WT and mutated IRES sites were shown in Figure S4C. WT IRES, but not the truncated or mutated IRES, exhibited the highest luciferase activity, indicating that the IRES sequences could induce 5′ cap-independent translation (Figure 4G). Driven by this IRES, circGlis3 could encode a putative protein of 348aa (termed Glis3-348aa), in which the unique C-terminal sequences were formed by spanning the backsplice junction (Figure 4E, red sequences).

To further validate the protein-coding ability of circGlis3, a circGlis3 overexpression plasmid containing a FLAG tag coding sequence upstream of the stop codon and a plasmid with defects in forming circRNA were constructed (Figure 4H). These plasmids were transfected into MIN6 cells and qRT-PCR assay verified that circGlis3 overexpression plasmid and circGlis3-Flag plasmid could express circGlis3 at high levels (Figure 4I). Besides, a specific antibody against the unique C-terminal sequence of Glis3-348aa was generated and the potential protein was detected by Western blot. The results showed that circGlis3-Flag plasmid produced a Flag-tagged protein, and the level of Glis3-348aa protein was elevated after the transfection of circGlis3 plasmid and circGlis3-Flag plasmid in MIN6 cells and mouse islets, indicating that circGlis3 was able to encode a protein (Figures 4J and S4D). To further confirm the existence of Glis3-348aa, circGlis3 was overexpressed in MIN6 cells and the amino acid sequences of Glis3-348aa was identified by MS. As predicted, an enhanced protein band of approximately 35 kDa was observed on the SDS-PAGE gel and the specific peptide fragments derived from Glis3-348aa was detected by MS (Figure 4K). In addition, consistent with the expression of circGlis3, the level of Glis3-348aa was significantly upregulated in palmitate-treated MIN6 cells and islets (Figures 4L and S4E). Similarly, Glis3-348aa levels were increased in the islets of *db/db* mice compared to *db/m* mice (Figure S4F). Overexpression of CELF1 enhanced Glis3-348aa levels in MIN6 cells and islets (Figures 4M and S4G). Altogether, these results demonstrate that circGlis3 encodes Glis3-348aa in β cells.

Glis3-348aa impairs β-cell function *in vitro*

To elucidate the biological functions of Glis3-348aa, we constructed a plasmid (circGlis3-ORF-Flag) containing the same ORF present in circGlis3 but in a linear formation and a mutant plasmid (circGlis3-ORF-Flag-mut) with the stop codon TAG deleted (Figure 5A). As anticipated,

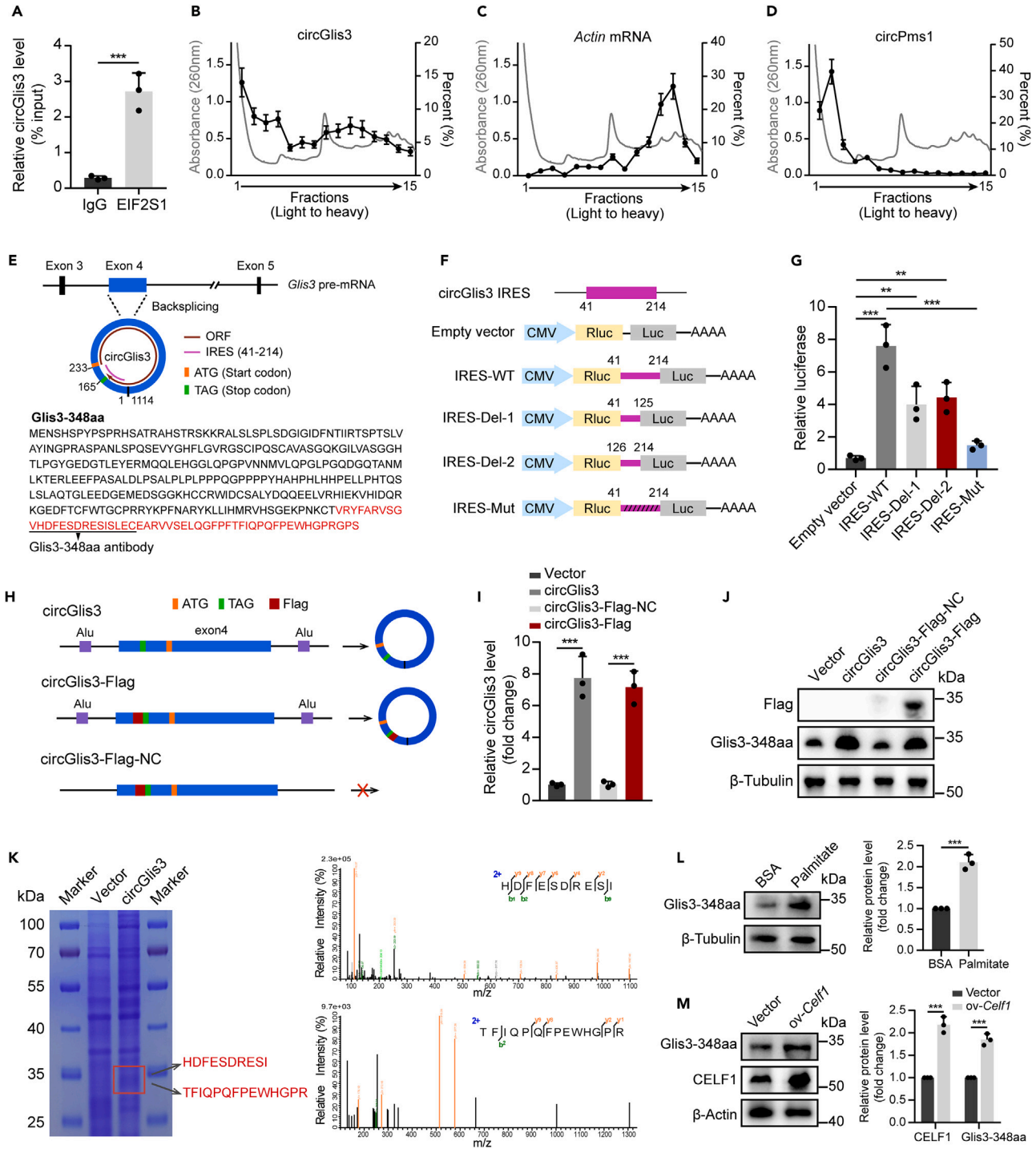

Figure 4. CircGlis3 encodes a 348-amino acid (aa) protein

(A) RIP assay was performed using anti-EIF2S1 antibody, followed by qRT-PCR to detect circGlis3 enrichment.

(B–D) The polysome fractions of MIN6 cells were extracted using 10%–45% sucrose gradient centrifugation, and absorbance at 260 nm was measured. The relative levels of circGlis3 (B), *Actin* mRNA (C), and circPms1 (D) were analyzed by qRT-PCR in gradient fractions in MIN6 cell lysates. *Actin* and circPms1 served as positive and negative controls, respectively.

(E) Top, the putative ORF, IRES and start/stop sites of circGlis3. Bottom, the amino acid sequences of Glis3-348aa encoded by the putative ORF, and specific amino acid sequences of Glis3-348aa are shown in red. The Glis3-348aa antibody was generated against the indicated sequences.

Figure 4. *Continued*

(F) Schematic illustration of five types of plasmids used for luciferase reporter assays. WT, a series of deletions of IRES sequences (IRES-Del-1, IRES-Del-2) and mutated IRES sequences (IRES-Mut) were inserted into the vector, respectively.

(G) The luciferase activity of Luc/Rluc was measured in the indicated five vectors. Luc, firefly luciferase; RLuc, renilla luciferase.

(H) Schematic of the expression constructs. CircGlis3 sequence was inserted into a circular RNA expression vector containing Alu elements to form circGlis3 plasmid. FLAG tag was added directly to upstream of the stop codon (TAG) to establish the circGlis3-Flag plasmid. The circGlis3-Flag sequence was cloned to a linear vector to form a negative control plasmid (circGlis3-Flag-NC).

(I and J) MIN6 cells were transfected with the indicated plasmids. The expression level of circGlis3 was analyzed by qRT-PCR (I), and the potential proteins were detected by Western blot (J).

(K) Total protein lysates from MIN6 cells transfected with circGlis3 plasmid or empty vector were separated by SDS-PAGE, followed by Coomassie brilliant blue staining. The differential gel bands near 35 kDa were excised and subjected to mass spectrometry to identify the specific sequences of Glis3-348aa.

(L) Western blot analysis of Glis3-348aa levels in MIN6 cells treated with BSA or palmitate.

(M) Western blot evaluated the levels of CELF1 and Glis3-348aa in MIN6 cells with CELF1 overexpression. Results are expressed as mean ± SD of three independent experiments. $^{**}p < 0.01$ and $^{***}p < 0.001$, by two-tailed Student's *t* test in (A, I, L, M), and one-way ANOVA (with Tukey post hoc test) in (G).

circGlis3-ORF-Flag plasmid produced a Flag-tagged protein and elevated the level of Glis3-348aa in MIN6 cells and mouse islets, while the circGlis3-ORF-Flag-mut plasmid did not (Figure 5B). In line with the previous results, the upregulation of Glis3-348aa significantly inhibited β-cell proliferation, cell viability and insulin secretion, and promoted β-cell apoptosis (Figures 5C–5H). Besides, a mutated IRES vector (circGlis3-IRESmut-Flag) was constructed by mutating IRES within the circGlis3-Flag plasmid. The results showed that both circGlis3-Flag and circGlis3-IRESmut-Flag plasmids dramatically enhanced the expression level of circGlis3 in MIN6 cells, whereas circGlis3-IRESmut-Flag plasmid failed to produce a Flag-tagged protein (Figures S5A and S5B). Similarly, overexpression of circGlis3-Flag significantly reduced β-cell viability and insulin secretion, and increased cell apoptosis, which could be partially abolished by mutating the IRES within circGlis3 (Figures S5C–S5E). Taken together, circGlis3 encodes Glis3-348aa to promote β-cell dysfunction *in vitro*.

Glis3-348aa interacts with GLIS3 protein and attenuates its transcriptional activity

We further explored the downstream mechanism by which Glis3-348aa contributed to β-cell dysfunction. IF assay revealed that Glis3-348aa was mainly located in the nucleus of MIN6 cells (Figure S6A). GLIS3 protein, which is encoded by the *Glis3* gene, is a transcription factor responsible for β-cell differentiation and insulin secretion.[36] The colocalization of Glis3-348aa and GLIS3 was observed in the nucleus of MIN6 cells (Figure 6A), and thus we wondered whether there was an interaction between Glis3-348aa and GLIS3 protein. Co-IP assays with anti-Glis3-348aa antibody showed that Glis3-348aa could interact with GLIS3 protein in MIN6 cells and mouse islets (Figures 6B and S6B). The interaction between Glis3-348aa and GLIS3 was further confirmed by Co-IP assays in MIN6 cells and islets transfected with HA-tagged GLIS3 plasmid or Flag-tagged circGlis3-ORF plasmid (Figures 6C, 6D, S6C, and S6D). Moreover, GLIS3 protein contains three known domains: an N-terminal conserved region (NCR), a DNA-binding domain (DBD) consisting of five zinc finger motifs, and a C-terminal transactivation domain (TAD) responsible for activating gene transcription, while Glis3-348aa lacks three zinc finger motifs and the transactivation domain, and possesses a distinct C-terminal instead (Figure S6E). HA-tagged recombinant GLIS3 plasmids with full-length (FL) or different forms of truncation were constructed and transfected into MIN6 cells (Figure 6E). Co-IP assays indicated that the TAD (743–935 aa) of GLIS3 protein was crucial for its interaction with Glis3-348aa (Figure 6F). Additionally, three-dimensional (3D) models of GLIS3 and Glis3-348aa were built using I-TASSER,[37] and molecular docking was performed using ZDOCK server.[38] Based on the predicted structures, Glis3-348aa was modeled with GLIS3 protein, and it appeared that the residues bound by Glis3-348aa were located in the C-terminal domain of GLIS3 protein (Figures S6E and S6F). These data suggest that Glis3-348aa forms a complex with GLIS3 protein by binding to its C-terminal TAD.

GLIS3 has been shown to directly regulate the transcription of targeted genes in β cells, including *Ins2*, *Ngn3,* and *Ccnd2*.[36,39] Of note, we found that the expression levels of *Ins2*, *Ngn3,* and *Ccnd2* were reduced by overexpressing circGlis3 in MIN6 cells and islets (Figure S6G and S6H). Given that Glis3-348aa bound to the C-terminal TAD of GLIS3 protein, we then wondered whether the transcriptional activity of GLIS3 was affected by Glis3-348aa. Luciferase plasmids containing the *Ins2*, *Ngn3,* and *Ccnd2* promoters were constructed respectively. Dual-luciferase reporter assays revealed that the promoter activities of *Ins2*, *Ngn3,* and *Ccnd2* were decreased by the overexpression of Glis3-348aa, whereas increased by the overexpression of GLIS3 (Figures 6G–6I). Furthermore, overexpression of Glis3-348aa markedly reduced the viability of MIN6 cells and inhibited the expression of *Ins2*, *Ngn3* and *Ccnd2* in MIN6 cells and islets, which could be restored by upregulating GLIS3 levels (Figures 6J, 6K, S6I, and S6J). Consistently, overexpressing GLIS3 reverted the decreased insulin content, reduced protein levels of NGN3 and CCND2, and increased levels of Cleaved caspase-3 induced by the elevation of Glis3-348aa in β cells (Figures 6L, 6M; S6K, and S6L). Collectively, our findings indicate that Glis3-348aa promotes β-cell dysfunction by interacting with GLIS3 and inhibiting its transcriptional activity.

Overexpression of circGlis3 promotes β-cell dysfunction *in vivo*

To verify whether the overexpression of circGlis3 also impairs β-cell function *in vivo*, we established a β cell-specific circGlis3 transgenic mouse model (Tg-circGlis3) by crossing homozygous circGlis3 knock-in mice with Ins2-Cre mice, and confirmed mouse genotypes by PCR (Figure S7A). qRT-PCR showed that circGlis3 was selectively overexpressed in the β cells of Tg-circGlis3 mice (Figures 7A and S7B). Metabolic analysis of mice revealed that the fasting blood glucose (FBG) level was significantly elevated by circGlis3 overexpression, whereas no

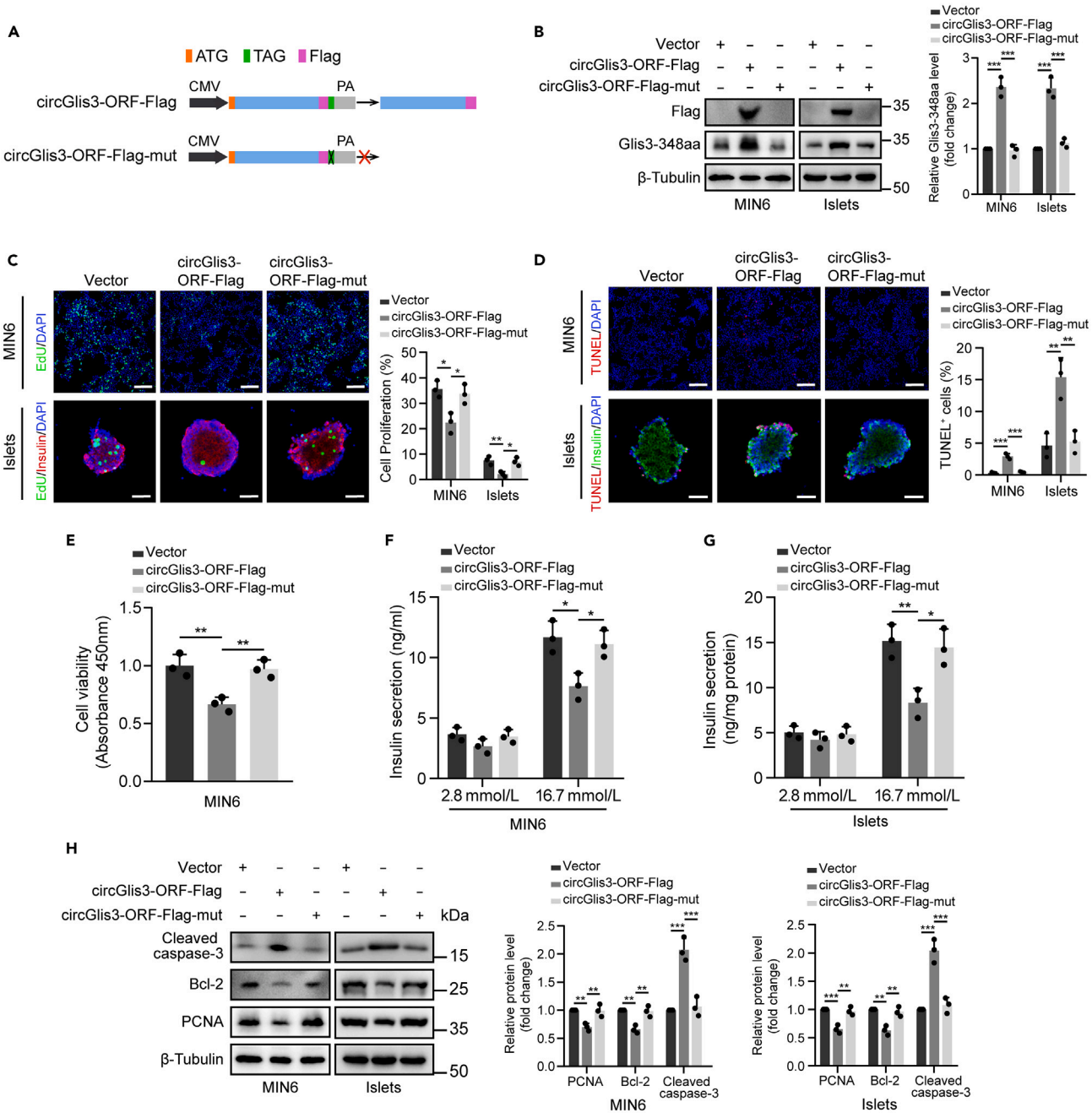

Figure 5. Glis3-348aa impairs β-cell function in vitro

(A) Schematic illustration of the circGlis3-ORF-Flag and circGlis3-ORF-Flag-mut constructs. The circGlis3 ORF sequence with FLAG tag was inserted into a linear expression vector to form circGlis3-ORF-Flag. The stop codon TAG was deleted in the mutant construct, which failed to produce a protein.

(B–H) MIN6 cells and primary mouse islets were transfected with the indicated plasmids. The expression levels of Flag and Glis3-348aa in MIN6 cells and islets were detected by Western blot (B). Cell proliferation in MIN6 cells (Scale bars represent 100 μm) and mouse islets (Scale bars represent 50 μm) was measured by EdU staining (C). Cell apoptosis in MIN6 cells (Scale bars represent 100 μm) and islets (Scale bars represent 50 μm) was evaluated by TUNEL staining (D). Cell viability of MIN6 cells was assessed by CCK-8 assay (E). Insulin secretion of MIN6 cells (F) and mouse islets (G) was measured by GSIS assay. Western blot analyzed the protein levels of PCNA, Bcl-2 and Cleaved caspase-3 in MIN6 cells and islets (H). Data are expressed as mean ± SD of three independent experiments. *p < 0.05, **p < 0.01 and ***p < 0.001, by one-way ANOVA (with Tukey post hoc test).

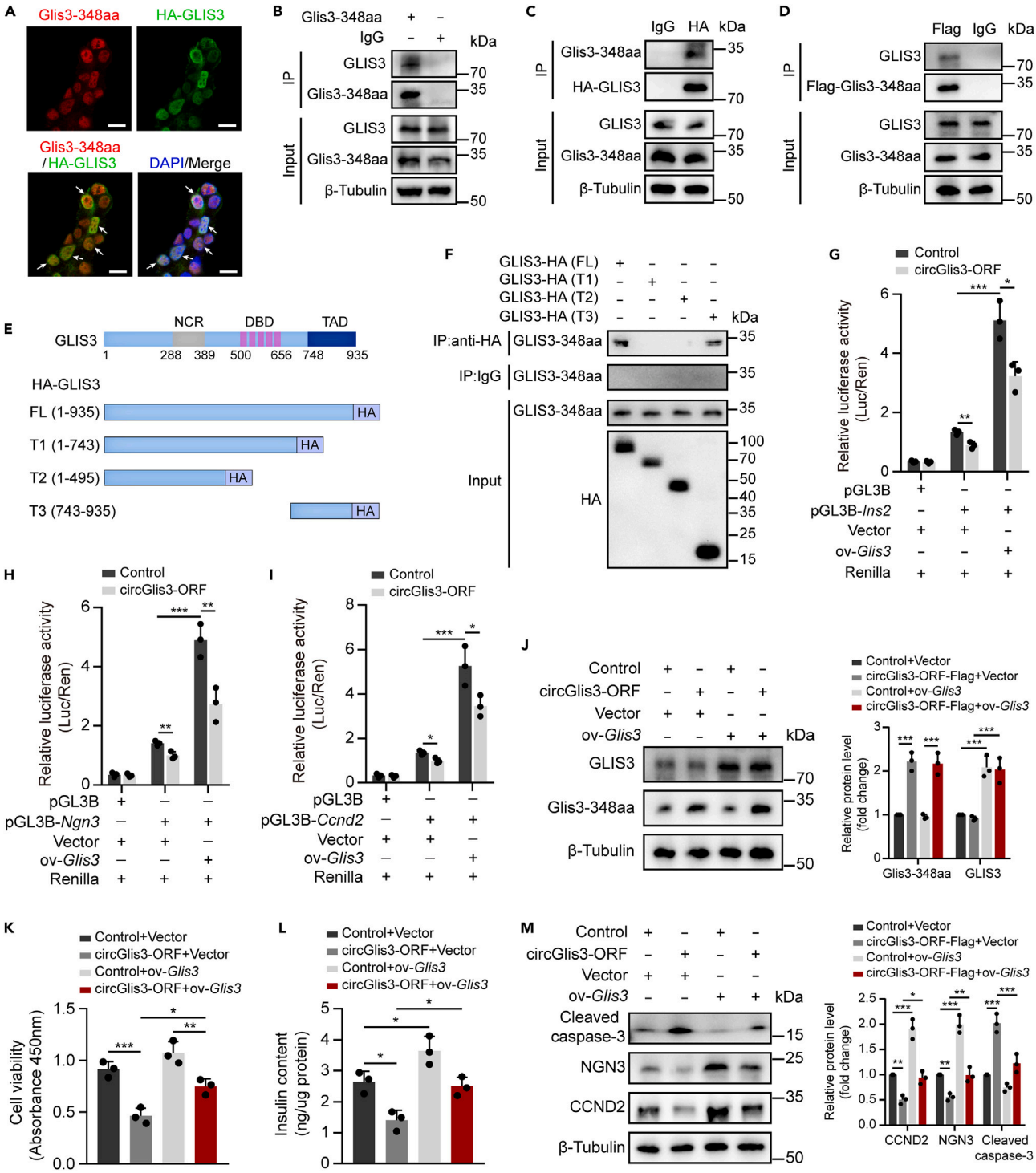

Figure 6. Glis3-348aa interacts with GLIS3 protein and attenuates its transcriptional activity

(A) IF assay showed the colocalization of Glis3-348aa and GLIS3 in MIN6 cells transfected with HA-tagged GLIS3. Scale bar, 10 μm.

(B) The interaction between Glis3-348aa and GLIS3 in MIN6 cells was analyzed by Co-IP assays using anti-Glis3-348aa antibody.

(C, D) Co-IP assays confirmed the interaction between Glis3-348aa and GLIS3 in MIN6 cells with overexpression of HA-GLIS3 (C) or Flag-Glis3-348aa (D).

(E) Schematic diagrams showing the construction of HA-tagged GLIS3 plasmids with full-length (FL) or different forms of truncation.

(F) MIN6 cells were transfected with plasmids encoding HA-tagged FL or truncated GLIS3, followed by Co-IP with anti-HA antibody.

Figure 6. *Continued*

(G–I) The circGlis3-ORF plasmid was generated by inserting circGlis3 ORF sequence into a linear expression vector. Luciferase plasmids containing the *Ins2*, *Ngn3* and *Ccnd2* promoters were constructed, respectively. MIN6 cells with overexpression of circGlis3-ORF were co-transfected with indicated plasmids, followed by detecting the promoter activity of *Ins2* (G), *Ngn3* (H) and *Ccnd2* (I) via dual-luciferase assays.

(J–M) MIN6 cells with circGlis3-ORF overexpression were transfected with pcDNA-*Glis3* plasmid (ov-*Glis3*) or empty vector (Vector). Western blot analyzed the protein levels of Glis3-348aa and GLIS3 (J). Cell viability was measured by CCK-8 assay (K). Insulin content was assessed by ELISA and normalized to total protein of cell lysates (L). Western blot detected the protein levels of CCND2, NGN3 and Cleaved caspase-3 (M). The Western blots images are representative of three independent experiments. Data are represented as mean ± SD of three independent experiments. *p < 0.05, **p < 0.01 and ***p < 0.001, by two-tailed Student's *t* test in (G-I), and one-way ANOVA (with Tukey post hoc test) in (J-M).

significant changes were noted in the body weight and random plasma glucose (RPG) between Tg-circGlis3 mice and WT littermates (Figures 7B, S7C, and S7D). Meanwhile, compared with control mice, the Tg-circGlis3 mice exhibited markedly impaired glucose tolerance and lower glucose-stimulated serum insulin levels (Figures 7C and 7D). Nevertheless, overexpression of circGlis3 had no significant effect on insulin sensitivity in Tg-circGlis3 mice (Figure S7E). In addition, a decreased proliferation rate and an increased apoptosis rate of β cells were observed in Tg-circGlis3 mice (Figures 7E and 7F). These results suggest that overexpression of circGlis3 leads to defective β-cell function *in vivo*.

To further confirm the underlying molecular mechanisms *in vivo*, we analyzed the expression levels of the downstream targets of circGlis3 in mouse islets. As anticipated, hnRNPF protein levels were reduced in the nucleus and elevated in the cytoplasm of islets from Tg-circGlis3 mice (Figure 7G). Likewise, SIRT1 levels were markedly decreased in the islets of Tg-circGlis3 mice, while the total protein level of hnRNPF did not change significantly (Figures 7H and S7F). Furthermore, the islets of Tg-circGlis3 mice exhibited a significant increase in Glis3-348aa levels and decrease in the expression levels of *Ins2, Ngn3,* and *Ccnd2* (Figures 7H and 7I). Besides, our previous study demonstrated that knockdown of circGlis3 by the injection of AAV8-shcircGlis3 ameliorated β-cell injury in high-fat diet (HFD)-induced diabetic mice.[17] We further validated that inhibiting circGlis3 in β cells of diabetic mice elevated hnRNPF protein levels in the nucleus and reduced hnRNPF protein levels in the cytoplasm (Figure 7J). Meanwhile, silencing circGlis3 upregulated SIRT1 protein levels and the expression levels of *Ins2*, *Ngn3*, and *Ccnd2* in the islets of diabetic mice, whereas reduced Glis3-348aa levels (Figures 7K and 7L).

DISCUSSION

Accumulating evidence has illustrated that circRNAs are aberrantly expressed in β cells under diabetic conditions and play important roles in the development of T2DM.[14–16] In this study, we identified that circGlis3, which was regulated by CELF1, promoted β-cell dysfunction by blocking the nuclear translocation of hnRNPF and encoding Glis3-348aa protein. Our findings not only uncover new mechanisms underlying circGlis3-induced β-cell dysfunction, but also provide new insights into the pathogenesis and treatment of T2DM.

Studies have shown that the biogenesis of circRNAs is modulated by specific *cis*-acting elements and *trans*-acting factors.[9,40] Some RBPs including QKI and HNRNPL have been reported to regulate the circularization and biogenesis of circRNAs.[18,19,41] Our study found that CELF1 promoted the formation of circGlis3 by binding to the flanked intron regions. CELF1, also known as CUGBP1, is a multifunctional RBP that regulates multiple stages of RNA processing.[26] It has been revealed that CELF1 was upregulated in the type 1 diabetic heart and contributed to aberrant alternative splicing patterns.[42] In addition, the islets of diabetic mice displayed elevated CELF1 levels, which attenuated insulin secretion via activating phosphodiesterase 3B.[43] Consistent with previous findings, our results demonstrated that CELF1 was upregulated in palmitate-treated β cells and the islets of diabetic mice. Moreover, overexpression of CELF1 increased β-cell apoptosis and reduced insulin secretion, indicating a critical role of CELF1 in β cells. However, the mechanisms underlying lipotoxicity-induced CELF1 overexpression requires further investigation.

CircRNAs, a class of covalently closed biomolecules, have been validated as key regulators of β-cell function.[14–16] Notably, our previous study illustrated that the expression level of circGlis3 was elevated in lipotoxic β cells and knockdown of circGlis3 could ameliorate β-cell injury in diabetic mice.[17] In this study, we established a transgenic mouse model with β cell-specific overexpression of circGlis3, and found that overexpression of circGlis3 impaired β-cell function *in vivo*. These findings provide new evidence supporting the detrimental role of circGlis3 in T2DM, and indicate that circGlis3 may be a potential therapeutic target for T2DM. In addition, circRNAs exhibit their effects in multiple ways, including sponging miRNAs, interacting with proteins and regulating gene transcription.[10,44] Here, we found that circGlis3 directly bound to hnRNPF protein to inhibit its nuclear translocation and the subsequent activation of *Sirt1* transcription, thereby leading to β-cell dysfunction, suggesting that circGlis3 can act as a decoy for hnRNPF protein to alter the cellular distribution of hnRNPF. Meanwhile, circGlis3 did not change the total protein level of hnRNPF, indicating that the binding of circGlis3 to hnRNPF has little effect on the translation or stability of hnRNPF. Besides, it is reported that the central glycine-tyrosine-arginine-rich (GYR) domain of hnRNPF harbors a nonclassical nuclear localization sequence that can interact with the import receptor transportin 1, facilitating the nuclear import of hnRNPF.[45] Our study identified that circGlis3 mainly bound to the qRRM2 motif of hnRNPF adjacent to the GYR domain. Therefore, it is reasonable to assume that the binding of circGlis3 to hnRNPF impedes the interaction between transportin 1 and hnRNPF, which warrants further exploration.

hnRNPF is an RNA-binding protein that participates in multiple processes of RNA metabolism, including alternative splicing, mRNA stabilization, and transcriptional regulation.[29] For example, hnRNPF was upregulated in bladder cancer and contributed to tumor metastasis by binding to the 3′ UTR of *Snail1* mRNA and enhancing its stability.[46] In addition, hnRNPF has been reported to be implicated in the kidney injury in diabetic mice by regulating the transcription of a series of genes, including *Sirt1* and *Ace2*.[30–34] Consistently, our study uncovered that in β cells, hnRNPF could activate the transcription of *Sirt1*, a NAD^+-dependent histone deacetylase that regulates insulin secretion and

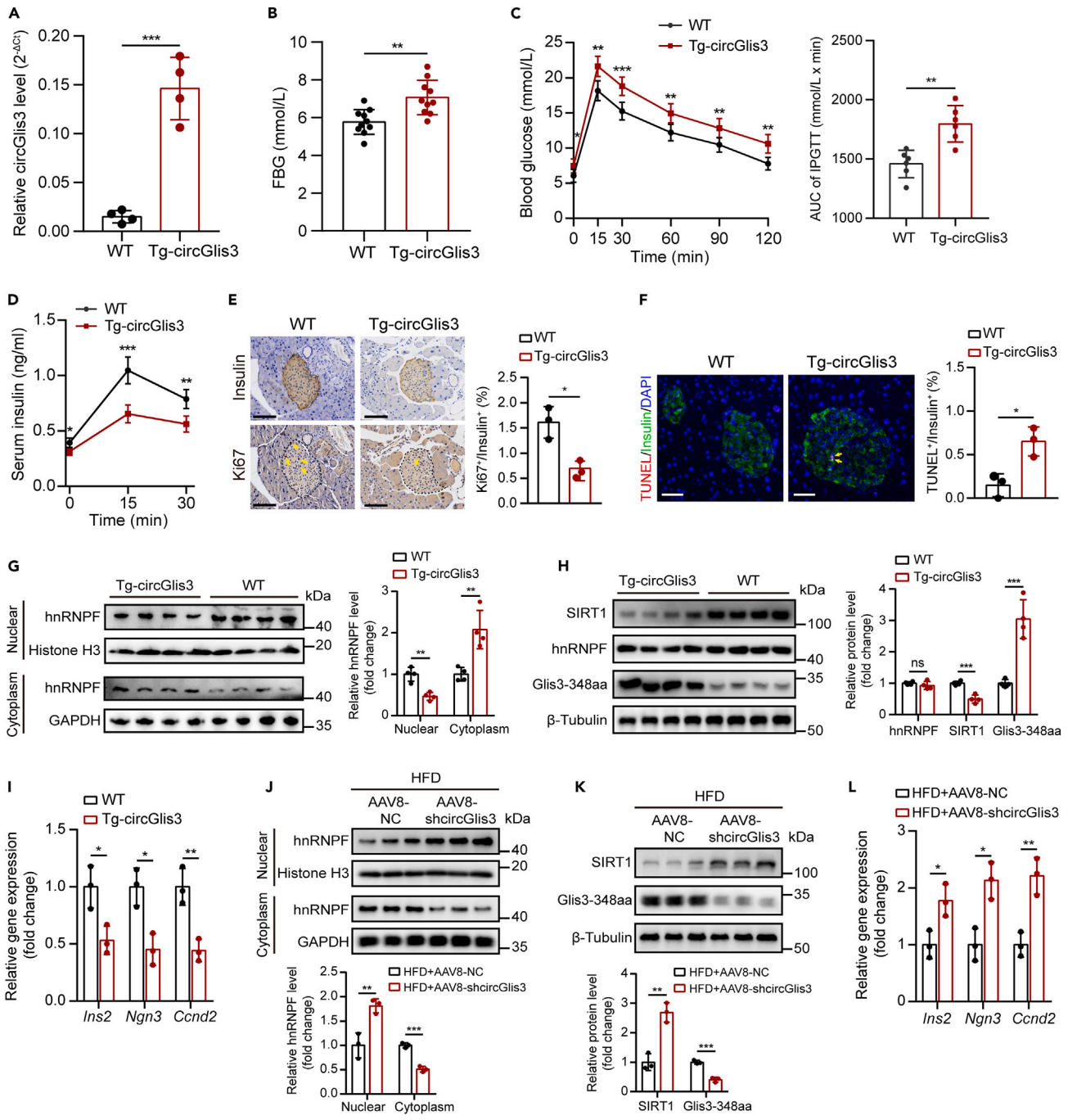

Figure 7. Overexpression of circGlis3 promotes β-cell dysfunction in vivo

(A) qRT-PCR analyzed the expression level of circGlis3 in the islets of Tg-circGlis3 mice and WT littermates (n = 4/group).

(B and C) FBG levels (B) and IPGTTs (C) of 12-week-old Tg-circGlis3 and control mice (*n* = 6–10/group).

(D) Whole blood samples of 12-week-old Tg-circGlis3 and control mice were taken at 0, 15 and 30 min after glucose injection, and serum insulin levels were measured (n = 5/group).

(E) IHC analysis of insulin and Ki67 expression in pancreatic sections from 14-week-old Tg-circGlis3 and control mice. Arrows indicate Ki67-positive β cells. Scale bar, 100 μm.

(F) β cell apoptosis was evaluated by TUNEL (red) and insulin (green) coimmunostaining. Arrows indicate the DAPI/TUNEL/insulin copositive β cells. Scale bar, 50 μm.

Figure 7. *Continued*

(G–I) The islets were isolated from 14-week-old Tg-circGlis3 and control mice. Western blot detected hnRNPF levels in the nucleus and cytoplasm of the islets (n = 4/group) (G). Western blot assessed the protein levels of SIRT1, hnRNPF and Glis3-348aa in the indicated mouse islets (n = 4/group) (H). qRT-PCR evaluated the expression levels of *Ins2*, *Ngn3* and *Ccnd2* in the islets (n = 3/group) (I).

(J–L) The islets were isolated from HFD-induced diabetic mice injected with AAV8-NC or AAV8-shcircGlis3. Western blot analyzed hnRNPF levels in the nucleus and cytoplasm of the islets (n = 3/group) (J). The protein levels of SIRT1 and Glis3-348aa in the islets were measured by Western blot (n = 3/group) (K). The expression levels of *Ins2*, *Ngn3* and *Ccnd2* were evaluated by qRT-PCR (n = 3/group) (L). Data are shown as mean ± SD of independent experiment indicated as above. *p < 0.05, **p < 0.01 and ***p < 0.001, ns indicates no significance, by two-tailed Student's *t* test.

promotes β-cell survival by deacetylating histones and a dozen nonhistone proteins.[47,48] Furthermore, we found that knockdown of hnRNPF induced β-cell dysfunction by reducing *Sirt1* expression levels, suggesting that hnRNPF may play an important role in maintaining β-cell function.

Recent studies have demonstrated that certain circRNAs could encode functional peptides/proteins.[35,49] As circRNA-encoded proteins share part of amino acid sequences with the cognate proteins and possess unique amino acid sequences, they are proposed to function as modulators of alternate protein complexes or dominant negative protein variants.[9] For instance, SHPRH-146aa encoded by circ-SHPRH functioned as a tumor suppressor by preventing the degradation of SHPRH protein.[50] Additionally, circARHGAP35 protein facilitated cancer progression, whereas ARHGAP35 protein played the opposite role,[18] indicating that some circRNA-encoded proteins could play independent or even opposite roles compared to their linear counterparts. Herein, we revealed that circGlis3 could encode a functional protein Glis3-348aa, and overexpression of Glis3-348aa promoted β-cell dysfunction. More importantly, Glis3-348aa directly bound to the C-terminal TAD of GLIS3 protein, which thereafter suppressed the transcriptional activity of GLIS3 and reduced the expression levels of target genes. GLIS3 is a critical transcription factor responsible for β-cell differentiation and insulin secretion.[36,51] Our study showed that Glis3-348aa, which lacks the TAD domain and has a distinct C-terminus, exerted a contrary biological function to GLIS3 protein. Hence, we think that the translation of circGlis3 represents a new mechanism for β-cell dysfunction in T2DM.

Conclusively, our study elucidates the molecular mechanism underlying circGlis3-induced β-cell dysfunction. CELF1 facilitates the biogenesis of circGlis3, which is upregulated in β cells under lipotoxic conditions. Moreover, circGlis3 impairs β-cell function through dual mechanisms. First, circGlis3 binds to hnRNPF protein and prevents its nuclear translocation, thereby inhibiting the transcription of *Sirt1*. Second, circGlis3 encodes Glis3-348aa that interacts with GLIS3 protein and suppresses its transcriptional activity. Our findings expand current knowledge on circRNAs function in T2DM pathogenesis and suggest circGlis3 as a potential therapeutic target for T2DM.

Limitations of the study

Most of the experiments in this study were conducted in rodent models (MIN6 cells, primary mouse islets and transgenic mice). Therefore, the use of human pancreatic islets for some key experiments may increase the translational impact of the current findings.

STAR★METHODS

Detailed methods are provided in the online version of this paper and include the following:

- KEY RESOURCES TABLE
- RESOURCE AVAILABILITY
  - Lead contact
  - Materials availability
  - Data and code availability
- EXPERIMENTAL MODEL AND STUDY PARTICIPANT DETAILS
  - Animals
  - Primary mouse islets
  - Cell culture studies
  - Study approval
- METHOD DETAILS
  - Metabolic studies
  - Quantitative real-time PCR (qRT-PCR)
  - Cell transfection
  - Lentivirus production and infection
  - Western blot
  - Cell viability analysis
  - EdU assay
  - TUNEL staining assay
  - Flow cytometric analysis
  - RNA fluorescence *in situ* hybridization (FISH)
  - Glucose-stimulated insulin secretion (GSIS) assay

- Immunofluorescence (IF)
- Immunohistochemistry (IHC)
- RNA-binding protein immunoprecipitation (RIP) assay
- Dual-luciferase reporter assay
- Co-immunoprecipitation (Co-IP) assay
- RNA pull-down assay and mass spectrometry analysis
- Polysome profiling

● QUANTIFICATION AND STATISTICAL ANALYSIS

SUPPLEMENTAL INFORMATION

Supplemental information can be found online at https://doi.org/10.1016/j.isci.2023.108680.

ACKNOWLEDGMENTS

This work was supported by the National Natural Science Foundation of China (Grant No. 82300908, 82200881), Guangdong Basic and Applied Basic Research Foundation (Grant No. 2023A1515012455, 202201011528), China Postdoctoral Science Foundation (Grant No. 2022M723647), the Project of Administration of Traditional Chinese Medicine of Guangdong Province (Grant No. 20211071), Science and Technology Projects in Guangzhou (Grant No. 202206010062), Shenzhen "Sanming Project" Research (Grant No. lc202002), and National Key Clinical Discipline.

AUTHOR CONTRIBUTIONS

Conceptualization, L.X., L.K., and Z.L.; methodology, L.X., Y.G., Z.L., and H.L., investigation, L.X., Y.G., Z.L., H.L., and L.H.; formal analysis, Z.Z., X.Z., and W.L.; resources, L.K., and Y.G.; writing—original draft, L.X., L.K., and Z.L.; writing-review and editing, L.X., L.K., Z.L., Y.G., and H.L.; funding acquisition, L.K., L.X., and Y.G.; supervision, L.K.; project administration, L.K.

DECLARATION OF INTERESTS

The authors declare no competing interests.

INCLUSION AND DIVERSITY

We support inclusive, diverse, and equitable conduct of research.

Received: April 17, 2023
Revised: October 12, 2023
Accepted: December 5, 2023
Published: December 9, 2023

REFERENCES

1. Taylor, R., Al-Mrabeh, A., and Sattar, N. (2019). Understanding the mechanisms of reversal of type 2 diabetes. Lancet Diabetes Endocrinol. *7*, 726–736.
2. Ježek, P., Jabůrek, M., Holendová, B., and Plecitá-Hlavatá, L. (2018). Fatty Acid-Stimulated Insulin Secretion vs. Lipotoxicity. Molecules *23*, 1483.
3. Hawley, J.A., Sassone-Corsi, P., and Zierath, J.R. (2020). Chrono-nutrition for the prevention and treatment of obesity and type 2 diabetes: From mice to men. Diabetologia *63*, 2253–2259.
4. Acosta-Montaño, P., and García-González, V. (2018). Effects of dietary fatty acids in pancreatic beta cell metabolism, implications in homeostasis. Nutrients *10*, 393.
5. Lytrivi, M., Castell, A.L., Poitout, V., and Cnop, M. (2020). Recent insights into mechanisms of beta-Cell lipo- and glucolipotoxicity in type 2 diabetes. J. Mol. Biol. *432*, 1514–1534.
6. Benito-Vicente, A., Jebari-Benslaiman, S., Galicia-Garcia, U., Larrea-Sebal, A., Uribe, K.B., and Martin, C. (2021). Molecular mechanisms of lipotoxicity-induced pancreatic beta-cell dysfunction. Int. Rev. Cell Mol. Biol. *359*, 357–402.
7. Ling, C., and Rönn, T. (2019). Epigenetics in Human Obesity and Type 2 Diabetes. Cell Metab. *29*, 1028–1044.
8. Singh, R., Chandel, S., Dey, D., Ghosh, A., Roy, S., Ravichandiran, V., and Ghosh, D. (2020). Epigenetic modification and therapeutic targets of diabetes mellitus. Biosci. Rep. *40*.
9. Kristensen, L.S., Andersen, M.S., Stagsted, L.V.W., Ebbesen, K.K., Hansen, T.B., and Kjems, J. (2019). The biogenesis, biology and characterization of circular RNAs. Nat. Rev. Genet. *20*, 675–691.
10. Misir, S., Wu, N., and Yang, B.B. (2022). Specific expression and functions of circular RNAs. Cell Death Differ. *29*, 481–491.
11. Nisar, S., Bhat, A.A., Singh, M., Karedath, T., Rizwan, A., Hashem, S., Bagga, P., Reddy, R., Jamal, F., Uddin, S., et al. (2021). Insights into the role of CircRNAs: Biogenesis, characterization, functional, and clinical impact in human malignancies. Front. Cell Dev. Biol. *9*, 617281.
12. Kristensen, L.S., Jakobsen, T., Hager, H., and Kjems, J. (2022). The emerging roles of circRNAs in cancer and oncology. Nat. Rev. Clin. Oncol. *19*, 188–206.
13. Salzman, J., Chen, R.E., Olsen, M.N., Wang, P.L., and Brown, P.O. (2013). Cell-type specific features of circular RNA expression. PLoS Genet. *9*, e1003777.
14. Haque, S., Ames, R.M., Moore, K., Lee, B.P., Jeffery, N., and Harries, L.W. (2020). Islet-expressed circular RNAs are associated with type 2 diabetes status in human primary islets and in peripheral blood. BMC Med. Genomics *13*, 64.
15. Stoll, L., Sobel, J., Rodriguez-Trejo, A., Guay, C., Lee, K., Venø, M.T., Kjems, J., Laybutt, D.R., and Regazzi, R. (2018). Circular RNAs as novel regulators of beta-cell functions in normal and disease conditions. Mol. Metab. *9*, 69–83.
16. Wu, L., Xiong, L., Li, J., Peng, Z., Zhang, L., Shi, P., Gong, Y., and Xiao, H. (2020). Circ-Tulp4 promotes beta-cell adaptation to lipotoxicity by regulating soat1 expression. J. Mol. Endocrinol. *65*, 149–161.

17. Xiong, L., Chen, L., Wu, L., He, W., Chen, D., Peng, Z., Li, J., Zhu, X., Su, L., Li, Y., et al. (2022). Lipotoxicity-induced circGlis3 impairs beta cell function and is transmitted by exosomes to promote islet endothelial cell dysfunction. Diabetologia *65*, 188–205.
18. Li, Y., Chen, B., Zhao, J., Li, Q., Chen, S., Guo, T., Li, Y., Lai, H., Chen, Z., Meng, Z., et al. (2021). HNRNPL circularizes ARHGAP35 to produce an oncogenic protein. Adv. Sci. *8*, 2001701.
19. Knupp, D., Cooper, D.A., Saito, Y., Darnell, R.B., and Miura, P. (2021). NOVA2 regulates neural circRNA biogenesis. Nucleic Acids Res. *49*, 6849–6862.
20. Armaos, A., Colantoni, A., Proietti, G., Rupert, J., and Tartaglia, G.G. (2021). CatRAPID omics v2.0: Going deeper and wider in the prediction of protein-RNA interactions. Nucleic Acids Res. *49*, W72–W79.
21. Moss, N.D., and Sussel, L. (2020). MRNA processing: An emerging frontier in the regulation of pancreatic beta cell function. Front. Genet. *11*, 983.
22. Magro, M.G., and Solimena, M. (2013). Regulation of beta-cell function by RNA-binding proteins. Mol. Metab. *2*, 348–355.
23. Alvelos, M.I., Juan-Mateu, J., Colli, M.L., Turatsinze, J.V., and Eizirik, D.L. (2018). When one becomes many-Alternative splicing in beta-cell function and failure. Diabetes Obes. Metab. *20*, 77–87.
24. Villate, O., Turatsinze, J.V., Mascali, L.G., Grieco, F.A., Nogueira, T.C., Cunha, D.A., Nardelli, T.R., Sammeth, M., Salunkhe, V.A., Esguerra, J.L.S., et al. (2014). Nova1 is a master regulator of alternative splicing in pancreatic beta cells. Nucleic Acids Res. *42*, 11818–11830.
25. Juan-Mateu, J., Rech, T.H., Villate, O., Lizarraga-Mollinedo, E., Wendt, A., Turatsinze, J.V., Brondani, L.A., Nardelli, T.R., Nogueira, T.C., Esguerra, J.L.S., et al. (2017). Neuron-enriched RNA-binding proteins regulate pancreatic beta cell function and survival. J. Biol. Chem. *292*, 3466–3480.
26. Xia, H., Chen, D., Wu, Q., Wu, G., Zhou, Y., Zhang, Y., and Zhang, L. (2017). CELF1 preferentially binds to exon-intron boundary and regulates alternative splicing in HeLa cells. Biochim. Biophys. Acta. Gene Regul. Mech. *1860*, 911–921.
27. Liu, H., Lan, T., Li, H., Xu, L., Chen, X., Liao, H., Chen, X., Du, J., Cai, Y., Wang, J., et al. (2021). Circular RNA circDLC1 inhibits MMP1-mediated liver cancer progression via interaction with HuR. Theranostics *11*, 1396–1411.
28. Wang, X., Xing, L., Yang, R., Chen, H., Wang, M., Jiang, R., Zhang, L., and Chen, J. (2021). The circACTN4 interacts with FUBP1 to promote tumorigenesis and progression of breast cancer by regulating the expression of proto-oncogene MYC. Mol. Cancer *20*, 91.
29. Geuens, T., Bouhy, D., and Timmerman, V. (2016). The hnRNP family: Insights into their role in health and disease. Hum. Genet. *135*, 851–867.
30. Miyata, K.N., Lo, C.S., Zhao, S., Zhao, X.P., Chenier, I., Yamashita, M., Filep, J.G., Ingelfinger, J.R., Zhang, S.L., and Chan, J.S.D. (2021). Deletion of heterogeneous nuclear ribonucleoprotein F in renal tubules downregulates SGLT2 expression and attenuates hyperfiltration and kidney injury in a mouse model of diabetes. Diabetologia *64*, 2589–2601.
31. Lo, C.S., Shi, Y., Chang, S.Y., Abdo, S., Chenier, I., Filep, J.G., Ingelfinger, J.R., Zhang, S.L., and Chan, J.S.D. (2015). Overexpression of heterogeneous nuclear ribonucleoprotein F stimulates renal Ace-2 gene expression and prevents TGF-beta1-induced kidney injury in a mouse model of diabetes. Diabetologia *58*, 2443–2454.
32. Lo, C.S., Shi, Y., Chenier, I., Ghosh, A., Wu, C.H., Cailhier, J.F., Ethier, J., Lattouf, J.B., Filep, J.G., Ingelfinger, J.R., et al. (2017). Heterogeneous nuclear ribonucleoprotein f stimulates sirtuin-1 gene expression and attenuates nephropathy progression in diabetic mice. Diabetes *66*, 1964–1978.
33. Ghosh, A., Abdo, S., Zhao, S., Wu, C.H., Shi, Y., Lo, C.S., Chenier, I., Alquier, T., Filep, J.G., Ingelfinger, J.R., et al. (2017). Insulin inhibits nrf2 gene expression via heterogeneous nuclear ribonucleoprotein F/K in diabetic mice. Endocrinology *158*, 903–919.
34. Ghosh, A., Zhao, S., Lo, C.S., Maachi, H., Chenier, I., Lateef, M.A., Abdo, S., Filep, J.G., Ingelfinger, J.R., Zhang, S.L., and Chan, J.S.D. (2019). Heterogeneous nuclear ribonucleoprotein f mediates insulin inhibition of Bcl2-Modifying factor expression and tubulopathy in diabetic kidney. Sci. Rep. *9*, 6687.
35. Li, H., Lan, T., Liu, H., Liu, C., Dai, J., Xu, L., Cai, Y., Hou, G., Xie, K., Liao, M., et al. (2022). IL-6-induced cGGNBP2 encodes a protein to promote cell growth and metastasis in intrahepatic cholangiocarcinoma. Hepatology *75*, 1402–1419.
36. Scoville, D.W., and Jetten, A.M. (2021). GLIS3: A critical transcription factor in islet beta-Cell generation. Cells *10*, 3471.
37. Zheng, W., Zhang, C., Li, Y., Pearce, R., Bell, E.W., and Zhang, Y. (2021). Folding non-homologous proteins by coupling deep-learning contact maps with I-TASSER assembly simulations. Cell Rep. Methods *1*, 100014.
38. Pierce, B.G., Wiehe, K., Hwang, H., Kim, B.H., Vreven, T., and Weng, Z. (2014). ZDOCK server: Interactive docking prediction of protein-protein complexes and symmetric multimers. Bioinformatics *30*, 1771–1773.
39. Jetten, A.M. (2018). GLIS1-3 transcription factors: Critical roles in the regulation of multiple physiological processes and diseases. Cell. Mol. Life Sci. *75*, 3473–3494.
40. Kramer, M.C., Liang, D., Tatomer, D.C., Gold, B., March, Z.M., Cherry, S., and Wilusz, J.E. (2015). Combinatorial control of Drosophila circular RNA expression by intronic repeats, hnRNPs, and SR proteins. Genes Dev. *29*, 2168–2182.
41. Conn, S.J., Pillman, K.A., Toubia, J., Conn, V.M., Salmanidis, M., Phillips, C.A., Roslan, S., Schreiber, A.W., Gregory, P.A., and Goodall, G.J. (2015). The RNA binding protein quaking regulates formation of circRNAs. Cell *160*, 1125–1134.
42. Belanger, K., Nutter, C.A., Li, J., Tasnim, S., Liu, P., Yu, P., and Kuyumcu-Martinez, M.N. (2018). CELF1 contributes to aberrant alternative splicing patterns in the type 1 diabetic heart. Biochem. Biophys. Res. Commun. *503*, 3205–3211.
43. Zhai, K., Gu, L., Yang, Z., Mao, Y., Jin, M., Chang, Y., Yuan, Q., Leblais, V., Wang, H., Fischmeister, R., and Ji, G. (2016). RNA-binding protein CUGBP1 regulates insulin secretion via activation of phosphodiesterase 3B in mice. Diabetologia *59*, 1959–1967.
44. Liu, C.X., and Chen, L.L. (2022). Circular RNAs: Characterization, cellular roles, and applications. Cell *185*, 2016–2034.
45. Van Dusen, C.M., Yee, L., Mcnally, L.M., and Mcnally, M.T. (2010). A glycine-rich domain of hnRNP H/F promotes nucleocytoplasmic shuttling and nuclear import through an interaction with transportin 1. Mol. Cell Biol. *30*, 2552–2562.
46. Li, F., Zhao, H., Su, M., Xie, W., Fang, Y., Du, Y., Yu, Z., Hou, L., and Tan, W. (2019). HnRNP-F regulates EMT in bladder cancer by mediating the stabilization of Snail1 mRNA by binding to its 3′ UTR. EBioMedicine *45*, 208–219.
47. Kitada, M., and Koya, D. (2013). SIRT1 in Type 2 Diabetes: Mechanisms and Therapeutic Potential. Diabetes Metab. J. *37*, 315–325.
48. Yu, L., Chen, J.F., Shuai, X., Xu, Y., Ding, Y., Zhang, J., Yang, W., Liang, X., Su, D., and Yan, C. (2016). Artesunate protects pancreatic beta cells against cytokine-induced damage via SIRT1 inhibiting NF-kappaB activation. J. Endocrinol. Invest. *39*, 83–91.
49. Lei, M., Zheng, G., Ning, Q., Zheng, J., and Dong, D. (2020). Translation and functional roles of circular RNAs in human cancer. Mol. Cancer *19*, 30.
50. Zhang, M., Huang, N., Yang, X., Luo, J., Yan, S., Xiao, F., Chen, W., Gao, X., Zhao, K., Zhou, H., et al. (2018). A novel protein encoded by the circular form of the SHPRH gene suppresses glioma tumorigenesis. Oncogene *37*, 1805–1814.
51. Scoville, D.W., Lichti-Kaiser, K., Grimm, S.A., and Jetten, A.M. (2019). GLIS3 binds pancreatic beta cell regulatory regions alongside other islet transcription factors. J. Endocrinol. *243*, 1–14.

STAR★METHODS

KEY RESOURCES TABLE

REAGENT or RESOURCE	SOURCE	IDENTIFIER
Antibodies		
Rabbit monoclonal anti-β-Tubulin	Cell Signaling Technology	Cat# 2128; RRID: AB_823664
Mouse monoclonal anti-GAPDH	Abcam	Cat# ab8245; RRID: AB_2107448
Rabbit monoclonal anti-β-Actin	Cell Signaling Technology	Cat# 4970; RRID: AB_2223172
Mouse monoclonal anti-CELF1	Novus	Cat# NB200-316; RRID: AB_2086153
Rabbit monoclonal anti-Bax	Abcam	Cat# ab32503; RRID: AB_725631
Rabbit monoclonal anti-Bcl-2	Cell Signaling Technology	Cat# 3498; RRID: AB_1903907
Rabbit polyclonal anti-Cleaved Caspase-3	Cell Signaling Technology	Cat# 9661; RRID: AB_2341188
Mouse monoclonal anti-PCNA	Cell Signaling Technology	Cat# 2586; RRID: AB_2160343
Rabbit polyclonal anti-hnRNPF	Novus	Cat# NBP1-33607; RRID: AB_2232974
Rabbit monoclonal anti-Histone H3	Cell Signaling Technology	Cat# 4499; RRID: AB_10544537
Mouse monoclonal anti-FLAG-Tag	Cell Signaling Technology	Cat# 8146; RRID: AB_10950495
Mouse monoclonal anti-SIRT1	Abcam	Cat# ab110304; RRID: AB_10864359
Rabbit polyclonal anti-EIF2S1	Abcam	Cat# ab70542; RRID: AB_1209560
Rabbit polyclonal anti-Glis3-348aa	NovoPro	Cat# NP29282
Rabbit polyclonal anti-GLIS3	Novus	Cat# NBP3-05128
Mouse monoclonal anti-HA-Tag	Abcam	Cat# ab1424; RRID: AB_301017
Rabbit monoclonal anti-CCND2	Cell Signaling Technology	Cat# 3741; RRID: AB_2070685
Rabbit polyclonal anti-NGN3	LifeSpan	Cat# LS-C332242
Mouse monoclonal anti-Insulin	Novus	Cat# NBP2-15195; RRID: AB_2893238
Rabbit polyclonal anti-Ki67	Abcam	Cat# ab15580; RRID: AB_443209
Bacterial and virus strains		
DH5a Chemically Competent Cell	Tsingke Biosciences	Cat# TSC-C14
Biological samples		
Mouse pancreas	This paper	N/A
Chemicals, peptides, and recombinant proteins		
Dulbecco's modified eagle medium (DMEM)	Gibco	Cat# C11995500BT
RPMI 1640 medium	Gibco	Cat# C11875500BT
Fetal bovine serum (FBS)	Gibco	Cat# 10270106
β-mercaptoethanol	Sigma-Aldrich	Cat# M3148
Antibiotics (P/S)	Gibco	Cat# 15140122
Trypsin-EDTA (0.25%)	Gibco	Cat# 25200072
TRIzol™ Reagent	Invitrogen	Cat# 15596018
Bovine serum albumin (BSA)	Sigma-Aldrich	Cat# B2064
Palmitate Acid (PA)	Sigma-Aldrich	Cat# P5585
Collagenase P	Roche	Cat# 1213873
Hank's balanced salt solution (HBSS)	Hyclone	Cat# SH30030.02
Lymphoprep™ Density gradient medium	StemCell	Cat# 07851
Krebs-Ringer bicarbonate HEPES buffer (KRBH)	Leagene	Cat# CZ0103
4% Paraformaldehyde (PFA)	Biosharp	Cat# BL539A
Triton X-100	Solarbio	Cat# T8200

(*Continued on next page*)

Continued

REAGENT or RESOURCE	SOURCE	IDENTIFIER
ProLong™ Gold (DAPI)	Invitrogen	Cat# P36935
RIPA Lysis Buffer	ThermoFisher	Cat# 89900
Lipofectamine™ 3000 Transfection Reagent	Invitrogen	Cat# L3000-015
Opti-MEM™ medium	Gibco	Cat# 31985070
Polyethyleneimine (PEI)	Proteintech	Cat# PR40001
Puromycin	Beyotime	Cat# ST551
Critical commercial assays		
PrimeScript™ RT reagent kit	Takara	Cat# RR014
TB Green® Premix Ex Taq™ II	Takara	Cat# RR820A
Mouse insulin ELISA kit	Mercodia	Cat# 10-1247-01
Pierce™ BCA protein assay kit	ThermoFisher	Cat# 23227
PARIS™ Kit	Invitrogen	Cat# AM1921
Cell Counting Kit-8	Dojindo	Cat# CK04
Cell Light EdU DNA imaging kit	RiboBio	Cat# C10310-3
One Step TUNEL apoptosis assay kit	Beyotime	Cat# C1090
Annexin V-FITC/propidium iodide (PI) apoptosis assay kit	Lianke	Cat# 70-AP101-100
Fluorescent *In Situ* Hybridization Kit	GenePharma	Cat# T24112
Magna RIP™ RNA-Binding Protein Immunoprecipitation Kit	Millipore	Cat# 17-700
Dual-Luciferase Reporter (DLR™) Assay System	Promega	Cat# E1910
Pierce Magnetic IP/Co-IP Kit	ThermoFisher	Cat# 88804
Pierce Magnetic RNA-Protein Pull-Down Kit	ThermoFisher	Cat# 20164
Deposited data		
Mass spectrometry data from RNA pull-down assays	This paper, PRIDE	Accession number: PXD037024
Mass spectrometry data from total protein lysates of MIN6 cells transfected with circGlis3	This paper, PRIDE	Accession number: PXD037447
Original western blot images	This paper, Mendeley	https://doi.org/10.17632/zt9z3txm54.1
Experimental models: Cell lines		
MIN6 cell	AddexBio	Cat# C0018008
293T cell	National Infrastructure of Cell Line Recource (NICR) of China	Cat# 1101HUM-PUMC000091
Experimental models: Organisms/strains		
Mouse: circGlis3$^{fl/fl}$: C57BL/6J	Cyagen Biosciences	N/A
Mouse: Ins2-Cre mice: B6.Cg-Tg (Ins2-cre)25Mgn/J	The Jackson Laboratory	JAX: 003573
Mouse: C57BL/6J	GemPharmatech Co., Ltd.	Cat# N000013
Mouse: db/db: BKS-Leprem2Cd479/Gpt	GemPharmatech Co., Ltd.	Cat# T002407
Oligonucleotides		
Primers for qPCR, see Table S3	This Paper	N/A
siRNA sequences, see Table S4	This Paper	N/A
Recombinant DNA		
pLKO.1–puro-circGlis3 shRNA	This paper	N/A
pLO5-ciR-circGlis3	Geneseed Biosciences	N/A
pLO5-ciR-circGlis3-Mut	Geneseed Biosciences	N/A
pcDNA3.1-hnRNPF-3×Flag	This paper	N/A
pcDNA3.1-Celf1	This paper	N/A

(*Continued on next page*)

Continued

REAGENT or RESOURCE	SOURCE	IDENTIFIER
pEZ-M01-Glis3-HA	GeneCopoeia Biosciences	N/A
pEZ-M01-circGlis3-ORF-Flag	GeneCopoeia Biosciences	N/A
circGlis3-IRES-Luciferase plasmid	VectorBuilder	N/A
Sirt1-pGL3 reporter vector	This paper	N/A
Ins2-pGL3 reporter vector	This paper	N/A
Ngn3-pGL3 reporter vector	This paper	N/A
Ccnd2-pGL3 reporter vector	This paper	N/A
Software and algorithms		
Graphpad Prism	Graphpad	https://www.graphpad.com/
ImageJ	ImageJ	https://ImageJ.nih.gov/ij/
Adobe Photoshop	Adobe	https://www.adobe.com/es/
SPSS 26.0	IBM	https://www.ibm.com/spss

RESOURCE AVAILABILITY

Lead contact

Further information and requests for resources and reagents should be obtained by contacting the lead contact, Liang Kang (kangl@mail.sysu.edu.cn).

Materials availability

This study did not generate new unique reagents.

Data and code availability

(1) Original Western blot images have been deposited at Mendeley and are publicly available as of the date of publication. The DOI is listed in the key resources table. Mass spectrometry data have been deposited to the ProteomeXchange Consortium via the PRIDE partner repository. Accession numbers are listed in the key resources table.
(2) This paper does not report original code.
(3) Additional information is available from the lead contact upon request.

EXPERIMENTAL MODEL AND STUDY PARTICIPANT DETAILS

Animals

A conditional circGlis3 knock-in transgenic mouse model on a C57BL6/J background (circGlis3$^{fl/fl}$ mice), in which circGlis3 and endogenous flanking sequence was targeted into the ROSA26 locus, was constructed by Cyagen Technology Company based on CRISPR/Cas9 technique. β-cell specific circGlis3 overexpression transgenic mice (Tg-circGlis3) were generated by crossing circGlis3$^{fl/fl}$ mice with Ins2-Cre mice (Jackson Laboratory). Wild-type (WT) littermates were used as control. Genotyping of Tg-circGlis3 mice was performed by PCR using the primers listed in Table S3. Metabolic studies were performed on 12-week-old Tg-circGlis3 and control mice. Ten-week-old male *db*/*db* mice (BKS-Lepr^{em2Cd479}/Gpt) and age-matched male littermate *db*/*m* mice were purchased from the Gempharmatech Co., Ltd (Jiangsu, China) and used for islet isolation. All of the mice were housed in standard specific pathogen-free conditions with a 12 h light/dark cycle and had free access to water and food.

Primary mouse islets

Pancreatic islets were isolated from Tg-circGlis3 mice, WT littermates, C57BL/6J mice, *db*/*db* and *db*/*m* mice at the indicated age. Briefly, collagenase P solution (Roche, Germany) was infused into the mouse pancreatic duct, and then the inflated pancreas was removed and digested in a water bath at 37°C for approximately 15 min. The tissue digestion was terminated with cold Hank's buffer, followed by density gradient centrifugation on a Histopaque gradient (StemCell Technologies, Canada) at 2400 rpm for 20 min. Finally, the islets were handpicked under a microscope and incubated in RPMI 1640 medium containing 10% FBS. 3–4 mice were used in each group.

Cell culture studies

MIN6 cells (AddexBio) were grown in DMEM (Gibco, USA) containing 25 mM D-glucose, 10 mM HEPES supplemented with 15% fetal bovine serum (FBS, Gibco), 50 μmol/L β-mercaptoethanol (Sigma-Aldrich, USA) and 1% penicillin/streptomycin (Gibco). 293T cells (National

Infrastructure of Cell Line Resource, NICR) were cultured in DMEM containing 10% FBS and 1% penicillin/streptomycin. All cells were cultured at 37°C in a humidified 5% CO2 atmosphere and were confirmed to be mycoplasma-free. For the palmitate (Sigma-Aldrich) treatment, MIN6 cells were incubated in medium containing 0.3 mmol/L palmitate or 0.3% (weight to volume) bovine serum albumin (BSA) for 24 h. Palmitate was prepared as previously described.[16]

Study approval

All of the animal experiments were approved by the Institutional Animal Care and Use Committee of Sun Yat-sen University and conformed to the Guide for the Care and Use of Laboratory Animals published by the National Institutes of Health.

METHOD DETAILS

Metabolic studies

Random plasma glucose (RPG) was tested in the free-feeding condition, and fasting blood glucose (FBG) was detected after overnight fasting. Intraperitoneal glucose tolerance tests (IPGTTs) and intraperitoneal insulin tolerance tests (IPITTs) were performed on Tg-circGlis3 mice and WT littermates as previously described.[17] For the IPGTTs, mice were fasted overnight and injected intraperitoneally with glucose (2 g/kg body weight). For the IPITTs, mice were intraperitoneally administered with insulin (1 U/kg body weight) after a 6-h fast. Blood glucose was measured at 0 (prior to glucose or insulin administration), 30, 60, 90 and 120 min after the glucose or insulin loading. In addition, mice whole bloods were taken at 0, 15 and 30 min after glucose injection, and the serum was collected by centrifugation at 3000 rpm for 10 min. Serum insulin levels were measured by the Ultra-Sensitive Mouse Insulin ELISA Kit (Mercodia, Sweden). 5–10 mice were used in each group.

Quantitative real-time PCR (qRT-PCR)

Total RNA was extracted using TRIzol reagent (Invitrogen), and RNA samples were reverse transcribed into cDNA using the PrimeScript RT reagent kit (TaKaRa, Japan). Quantitative real-time PCR (qRT-PCR) assays were subsequently carried out on an ABI 7500 real-time PCR system (Applied Biosystems, USA) with TB Green Premix Ex Taq II (TaKaRa) according to the manufacturer's instructions. RNA levels were determined by $2^{-\Delta\Delta Ct}$ methodology and normalized to *β-Actin*. The primer sequences are listed in Table S3.

Cell transfection

CircGlis3 plasmid was generated by cloning *Glis3* exon 4 into pLO5-ciR vector (Geneseed, Guangzhou, China). hnRNPF and CELF1 overexpression plasmids were constructed by inserting the full length of *hnRNPF* ORF and *Celf1* ORF into pcDNA3.1 vector, respectively. Scramble siRNA and siRNAs targeting circGlis3, hnRNPF or the indicated RBPs were purchased from GenePharma (Shanghai, China). The transfection of plasmids or siRNAs was conducted by Lipofectamine 3000 (Invitrogen) following the manufacturer's instructions. Details of the siRNAs are shown in Table S4.

Lentivirus production and infection

pLKO.1-based circGlis3 shRNA or pLO5-ciR-circGlis3 plasmid was cotransfected with packaging plasmids psPAX2 and pMD2.G (Addgene, USA) into 293T cells using polyethyleneimine (Proteintech, China). Virus particles were harvested after 48 h of transfection, and then added into the plate to infect MIN6 cells. Infection efficiency was evaluated by qRT-PCR.

Western blot

MIN6 cells or islets were lysed in RIPA lysis buffer (Invitrogen, USA) containing a protease inhibitor cocktail (Promega, USA) to extract total protein. Protein samples were separated by SDS-PAGE (10%) and electrically transferred to polyvinylidene fluoride (PVDF) membranes. The membranes were blocked with 5% milk, and then incubated overnight with the respective antibodies (refer to Table S5 for details) at 4°C. Next, the membranes were washed with TBST and incubated with secondary antibodies for 1 h. The bands were detected using enhanced chemiluminescence (Millipore, USA) and analyzed by the Bio-Rad electrophoresis image analyzer.

Cell viability analysis

MIN6 cells were seeded in 96-well plates at 1×10^4 cells per well (five replicate wells) overnight and then received indicated treatments. Cell viability was assessed by Cell Counting Kit-8 (CCK-8) (Dojindo, Japan) following the manufacturer's instructions. The absorbance was read at 450 nm using a microplate reader (Bio-Rad, USA).

EdU assay

Cell proliferation was determined using the Cell Light EdU DNA imaging kit (RiboBio, Guangzhou, China) according to the manufacturer's protocol. Briefly, MIN6 cells or mouse islets were seeded in confocal dishes at a certain density. Then, cells were incubated with 50 μM EdU labeling medium for 2.5 h. Following this, the cells were fixed with 4% paraformaldehyde for 30 min, permeabilized with 0.5% Triton X-100 for 15 min, and incubates with Apollo fluorescent dye for 30 min. Finally, DAPI was applied to stain the nuclei. Images were captured by Leica TCS SP8 Confocal Microscope system (Leica, Germany), and the percentage of EdU positive cells was analyzed by ImageJ software.

TUNEL staining assay

TUNEL staining of MIN6 cells or islets was conducted using the One Step TUNEL apoptosis assay kit (Beyotime, Shanghai, China) according to the manufacturer's instructions. Briefly, MIN6 cells or mouse islets were seeded in confocal dishes and received indicated treatments. Then, cells were fixed with 4% paraformaldehyde for 30 min, permeabilized with 0.5% Triton X-100 for 10 min, and incubated with TUNEL reaction mixture for 1 h. DAPI was used to stain the nuclei. Images were acquired with a confocal microscopy (Leica), and the apoptosis rate was analyzed by ImageJ software.

Flow cytometric analysis

Cell apoptosis was assessed using Annexin V-FITC/propidium iodide (PI) apoptosis assay kit (Lianke, Hangzhou, China) following the protocols. Briefly, MIN6 cells with different treatments were harvested, washed with PBS, and then incubated with Annexin V-FITC and PI staining solution for 10 min in the dark. Cell apoptosis data were obtained with flow cytometry (BD FACS Calibur, USA) and analyzed by Flow Jo v.10.0.7 software (Tree Star, USA).

RNA fluorescence *in situ* hybridization (FISH)

The Cy3-labeled circGlis3 probe (5′-CTCTTGCAAAATAACGGACCGTACACTTGTTGGGCTTC-3′) was designed and synthesized by GenePharma (Shanghai, China). FISH assay was performed using Fluorescent *In Situ* Hybridization Kit (GenePharma) according to the manufacturer's instructions. Briefly, MIN6 cells were fixed with 4% paraformaldehyde for 20 min, permeabilized with 0.1% Buffer A for 20 min, and incubated with 2×Buffer C for 20 min. The probe solution (4μM) was denatured by heating at 73°C for 5 min before being added to the cells, and then incubated overnight at 37 °C in the dark. Following this, cells were washed with preheated 0.1% Buffer F, 2×Buffer C and 1×Buffer C successively. DAPI was used to stain the nuclei. Images were obtained with a confocal microscopy (Leica).

Glucose-stimulated insulin secretion (GSIS) assay

GSIS assays were conducted in MIN6 cells and primary mouse islets. Briefly, MIN6 cells were seeded in 48-well plates at 5×10^4 cells per well, and mouse islets were seeded in 48-well plates at 30 islets per well. After indicated treatments, the medium was removed and cells were incubated in HEPES-balanced Krebs-Ringer bicarbonate buffer (KRBH) with low glucose (2.8 mmol/L) for 1 h. Then, the supernatants were collected and cells were washed with KRBH buffer, followed by incubation with KRBH containing stimulatory glucose (16.7 mmol/L) for 1 h. The supernatants were collected again and the cell number was recalculated. The results for MIN6 cells were expressed as the concentration of insulin secreted per 5×10^4 cells. The insulin secretion level of mouse islets was normalized to the total cellular protein content.

Immunofluorescence (IF)

MIN6 cells or mouse pancreas frozen sections were fixed in 4% paraformaldehyde, then permeabilized with 0.5% Triton X-100 for 30 min, and blocked with 5% BSA for 1 h. Immunostaining was conducted by incubating MIN6 cells or sections with primary antibodies (anti-hnRNPF, anti-HA, anti-Glis3-348aa and anti-Insulin) respectively at 4°C overnight. Then, MIN6 cells or sections were incubated with secondary antibody (Alexa Fluor 594 or 488-conjugated IgG) at room temperature for 1 h, and DAPI was used to visualize the nuclei. Images were photographed using a confocal microscope (Leica, Germany). Details of antibodies used here are presented in Table S5.

Immunohistochemistry (IHC)

Pancreas tissues of Tg-circGlis3 mice and WT littermates were fixed with 4% paraformaldehyde and then embedded in paraffin and cut into slices. For immunohistochemical analysis, paraffin sections were incubated with antibodies against Ki67 or Insulin, followed by incubating with secondary antibodies. DAB complex was used as the chromogen and the nuclei were counterstained with hematoxylin. Images were captured at identical exposure conditions using a microscope (Leica, Germany).

RNA-binding protein immunoprecipitation (RIP) assay

Flag-tagged hnRNPF plasmids with full-length (FL) or different forms of truncation were constructed and transfected into MIN6 cells, respectively. RIP assay was carried out by Magna RIP RNA-Binding Protein Immunoprecipitation Kit (Millipore) according to the instructions. Briefly, MIN6 cells were collected with RIP lysis buffer. The cell lysate was incubated overnight with protein A/G beads and specific antibodies at 4°C. Then, the beads were pelleted and washed with RIP buffer, followed by elution of the coprecipitated RNAs. Total RNA from each sample was reverse transcribed into cDNA, and the enrichment of the RNA co-immunoprecipitated with indicated antibody was analyzed by qRT-PCR. Details of antibodies used here are shown in Table S5.

Dual-luciferase reporter assay

The promoter sequences of *Sirt1*, *Ins2*, *Ngn3* and *Ccnd2* were synthesized and cloned into the luciferase reporter plasmid pGL3-basic vector, respectively. The full length of hnRNPF ORF and GLIS3 ORF were inserted into pcDNA3.1 vector, respectively. *Sirt1*-pGL3 reporter vector, hnRNPF plasmid and pRL-TK vector (Promega, USA) were co-transfected into MIN6 cells using Lipofectamine 3000 (Invitrogen). Besides, *Ins2*-pGL3 reporter vector, *Ngn3*-pGL3 reporter vector and *Ccnd2*-pGL3 reporter vector were co-transfected with GLIS3 plasmid and pRL-TK

vector into MIN6 cells, respectively. The luciferase activity was measured by the Dual-Luciferase Reporter Assay System (Promega, USA) on an Infinite F500 Multimode plate reader (TECAN, Austria) and each sample was detected in triplicate.

The plasmids, of which the renilla luciferase (Rluc) was placed in front and the firefly luciferase (Luc) was placed in the back, were constructed by VectorBuilder (Guangzhou, China). The sequences of potential IRES, truncation mutant or IRES with point mutation were amplified and inserted into the middle of Rluc and Luc. The plasmids were transfected into MIN6 cells and the luciferase activity was evaluated as described above. The results were shown as relative Luc/Rluc activity.

Co-immunoprecipitation (Co-IP) assay

MIN6 cells or primary mouse islets were lysed in lysis buffer on ice for 30 min, and then purified by centrifugation for 15 min at 4°C. The supernatants were incubated with antibodies specific for Flag or HA at 4°C for 1 h, followed by incubating with protein A beads (Invitrogen, USA) at 4°C for 2 h. Then the beads were washed twice with lysis buffer, and 2×SDS buffer were then added for elution (100°C, 10 min). Samples were obtained by centrifugation and used for Western blot analysis.

RNA pull-down assay and mass spectrometry analysis

RNA pull-down assay in MIN6 cells was performed by using Pierce Magnetic RNA-Protein Pull-Down Kit (Thermo Scientific, Waltham, MA, USA) as previously described.[17] The circGlis3-interacting proteins were analyzed by mass spectrometry (MS) and further validated by Western blot. The MS analysis was performed on Q Exactive hybrid quadrupole-Orbitrap mass spectrometer (Thermo Scientific, USA). Protein identification was performed with MASCOT software (v2.3.0) by searching Uniprot_*Aedis Aegypti* with the following parameter settings: peptide mass tolerance set to 20 ppm, one missed trypsin cleavage allowed, MS/MS fragment tolerance set to 0.6 Da, significance threshold set to 0.05. For each protein match, MASCOT calculates an overall protein score. This number reflects the combined scores of all observed mass spectra that can be matched to amino acid sequences within that protein. A higher score indicates a more confident match. MS data are available via ProteomeXchange with identifier PXD037024. The differential proteins identified by MS between circGlis3 and linear transcript pull-down groups are listed in Table S2.

In addition, total protein lysates from MIN6 cells transfected with circGlis3 plasmid or empty vector were separated via SDS-PAGE, and then the gels were stained with Coomassie brilliant blue (Beyotime, China). The differential gel bands near 35 kDa were excised and analyzed by MS to identify the specific sequences of Glis3-348aa. MS data are available via ProteomeXchange with identifier PXD037447.

Polysome profiling

Polysome profiling was carried out according to a previous study.[18] MIN6 cells were treated with cycloheximide and incubated at 37°C for 3 min. Then cells were lysed in lysis buffer containing 10 mM MgCl2, 10 mM NaCl, 10 mM Tris-HCl pH 7.5, 1% sodium deoxycholate, 1% Triton X-100, 1 mM DTT, 0.1 mg/mL cycloheximide, and 0.2 U/μL RNase inhibitor. The samples were immediately placed on ice, followed by centrifugation at 16000 *g* for 5 min to pellet the nuclei and cellular debris. Linear sucrose gradients were prepared with a Gradient Master (Biocomp, Canada). Cytoplasmic lysates were loaded into 10%–45% sucrose gradients and separated by ultracentrifugation with an SW41 rotor (Beckman, USA) at 4°C, 274000 g for 100 min. Fractions were collected by a BioComp Piston Gradient Fractionator equipped with a Bio-Rad Econo UV Monitor (set at 260 nm). RNA isolated from each fraction was extracted with Trizol-LS (Invitrogen) and analyzed by qRT-PCR following the manufacturer's instruction.

QUANTIFICATION AND STATISTICAL ANALYSIS

All experiments were conducted at least three times unless otherwise noted, and all data are presented as mean ± SD. Two-tailed Student's *t* test for two groups and one-way ANOVA (followed by Tukey's post hoc test) for multiple groups were used to determine the statistical significance. Statistical analyses were performed using GraphPad Prism 8.0 software or SPSS 26.0 software (SPSS, USA). A p value <0.05 was considered statistically significant.